Mll1 pioneers histone H3K4me3 deposition and promotes formation of CD8$^+$ T stem cell memory

Authors: Adam J. Getzler[1,2], Megan A. Frederick[1#], Justin J. Milner[3%], Thomas Venables[1], Huitian Diao[1,2$], Clara Toma[3], Shashank D. Nagaraja[1,2], Dominic S. Albao[1,2], Simon Bélanger[4], Shanel M. Tsuda[1,2], Jihye Kim[1], Shane Crotty[4], Ananda W. Goldrath[3] and Matthew E. Pipkin[1]*

Affiliations:

[1] Department of Immunology and Microbiology, The Herbert Wertheim UF Scripps Institute for Biomedical Innovation & Technology, Jupiter, FL.

[2] The Skaggs Graduate Program in Chemical and Biological Sciences at Scripps Research, Jupiter, FL

[3] Division of Biological Sciences, University of California, San Diego, La Jolla, California, USA

[4] Division of Vaccine Discovery, The La Jolla Institute of Allergy and Immunology, La Jolla, CA

[#]Current address: Department of Cell and Developmental Biology, University of Pennsylvania, Perelman School of Medicine, Philadelphia, PA

[$]Current address: BioNTech US, Cambridge, MA

[%]Current address: Lineberger Cancer Center, University of North Carolina, Chapel Hill, NC

Current address: Vir Biotechnology, San Francisco, CA

*Correspondence to: m.pipkin@ufl.edu

Abstract: CD8$^+$ T cells with stem cell-like properties (T_{SCM}) sustain adaptive immunity to intracellular pathogens and tumors. However, the developmental origins and chromatin regulatory factors (CRFs) that establish their differentiation are unclear. Using an RNA interference screen of all CRFs we discovered the histone methylase Mll1 was required during T cell receptor (TCR) stimulation for development of a T_{SCM} precursor state and mature memory (T_{MEM}) cells, but not short-lived or transitory effector cell-like states, in response to viral infections and tumors. Mll1 was essential for widespread *de novo* deposition of histone H3 lysine 4 trimethylation (H3K4me3) upon TCR stimulation, which accounted for 70% of all activation-induced sites in mature T_{MEM} cells. Mll1 promoted both H3K4me3 deposition and reduced TCR-induced Pol II pausing at genes whose single-cell transcriptional dynamics explained trajectories into nascent T_{SCM} precursor states during viral infection. Our results suggest Mll1-dependent control of Pol II elongation and H3K4me3 establishes and maintains differentiation of CD8$^+$ T_{SCM} cell states.

Introduction:

Naive CD8 T cells activated by T cell receptor (TCR), co-receptor and cytokine stimulation during infections or cancer develop transcriptionally heterogeneous cell states (*1-5*) that give rise to diverse effector (T_{EFF}), memory (T_{MEM}), exhausted (T_{EX}) and dysfunctional (T_{DYS}) cell phylogenies (*6-10*). During acutely resolved infections in which antigen exposure is episodic, protective T_{EFF} and T_{MEM} cells develop (*8, 11*). Memory stem cells (T_{SCM}) that develop after acute infection are an incompletely defined subset of central memory (T_{CM}) T cells that highly express the transcription factor (TF) Tcf1 (encoded by *Tcf7*), re-express some naive cell attributes and sustain adaptive immunity by self-renewing under homeostatic conditions. In response to secondary infection, T_{SCM} cells proliferate most extensively and regenerate the compendium of protective T_{EFF} and T_{MEM} cell populations (*12-17*). These functions might explain the capacity of T_{MEM} cells to survive and proliferate to extents that exceed individual organismal lifespans (*18*). During chronic infections and cancer, subsets of "stem-like" progenitor T_{SCM}-like cells (termed exhausted progenitor (T_{EX}^{prog}) cells) persist in the face of chronic antigen exposure and differentiate into transitory T_{EFF}-like (T_{EX}^{trans}) cells that sustain the T cell response and curb pathogen or tumor loads (*19, 20*), but which progressively lose function and become terminally "exhausted" (T_{EX}^{term}) or "dysfunctional" (*21-27*). Differential chromatin remodeling correlates with the formation of distinct CD8 T cell states (*28-31*), but the transcriptional mechanics that create gene expression heterogeneity in TCR stimulated cells and establish their early developmental trajectories are incompletely understood. Moreover, while chromatin regulatory factors (CRFs) that silence genes which promote the longevity of T_{MEM} and that enforce terminal differentiation of T_{EFF} cells have been identified (*32-35*), those which establish transcriptional competence and promote formation of long-lived stem cell-like memory are still unknown.

Results:

Identification of CRFs that coordinately regulate expression of PD-1, LAG3, TIM3 and Id3.

Very early after either acute or chronic lymphocytic choriomeningitis virus (LCMV) infection, activated CD8 T cell populations that most highly express the transcriptional regulators Id3 and Tcf1 (encoded by *Tcf7*) have an enhanced capacity to develop into T_{SCM} or T_{EX}^{prog} cells compared to T_{EFF} or T_{EX} cells (*2, 36*). In either infectious context, TCR activated cells initially uniformly induce cell surface expression of the co-inhibitory receptors PD-1 (*Pdcd1*), Lag3 (*Lag3*) and Tim3 (*Havcr2*) (*37*), but only those responding to chronic infection increase and sustain their expression (*2, 36, 37*). We hypothesized that CRFs which coordinately regulated expression of Id3, and the T_{EX} cell markers PD-1, Lag3 and Tim3 following initial TCR stimulation, might also more generally control the early formation of T_{SCM} and T_{EX}^{prog} cells as opposed to more terminally differentiated T_{EFF} or T_{EX} cells. To screen for these CRFs, a library of retrovirally expressed microRNA30-embedded short-hairpin RNAs (shRNAmirs) targeting all murine CRFs was constructed and naive LCMV-specific (P14) CD8 T cells activated via TCR signals were transduced with individual shRNAmirs in separate wells (Fig 1A). The expression of nine cell surface receptors and a GFP reporter allele in the endogenous *Id3* locus (Id3-GFP) was monitored in shRNAmir-transduced cells, and the average loss-of-function effects on expression of these T cell differentiation markers derived from multiple, unique shRNAmirs targeting each CRF in the separate wells were summarized (RNAi-effects) and ranked (fig S1, table S1). We performed two orthogonal screens: The first examined surface receptor expression on P14 cells 6 days after primary TCR-activation and culture with interleukin-2 (IL-2) under conditions that promote key aspects of differentiation into effector (IL-2^{hi}) or memory (IL-2^{lo}) cells (Fig 1B *right*, fig S1A-B, table S1)(*38*); the second analyzed P14 *Id3*-GFP CD8 T cells 3 days after primary TCR stimulation (two days after transduction) and focused on expression of *Id3*-GFP, PD-1 and Lag3 (Fig 1B *left*, fig S1A-B, table S1).

Multiple genes encoding CRF subunits that assemble into the same biochemical complexes exhibited analogous RNAi-effects, such that suppressing each CRF either increased (positive RNAi-effect) or decreased (negative RNAi-effect) expression of PD-1, Lag3, Tim3 or *Id3*-GFP (fig S1C, table S1). Genes encoding the COMPASS-family of histone methyltransferase complexes (*39*), MOZ/MOF acetyltransferases, NuRD and polycomb group (PcG) proteins were significantly enriched among all CRFs with positive PD-1 RNAi-effects, whereas genes encoding BAF complex subunits were enriched among CRFs with negative PD-1 RNAi-effects (Fig 1B, fig S1B-C). In addition, CRFs with positive PD-1 RNAi-effects positively correlated with those that exhibited positive Lag3 or Tim3 RNAi-effects, and modestly correlated with those that had negative RNAi-effects on *Id3*-GFP (fig S1D). Thus, multiple distinct CRFs that assemble in shared complexes regulated the coordinated, and reciprocal, expression of co-inhibitory receptors and *Id3*-GFP upon naive CD8 T cell activation.

Individual CRFs were prioritized by focusing on those whose depletion had both the strongest effects and coordinately increased or decreased expression of more than one co-inhibitory receptor (Fig 1B and fig S1B, top/bottom 15% of RNAi-effects, table S1). Depletion of Mll1, the catalytic subunit of Mll-COMPASS-like complexes (encoded by *Kmt2a*), increased expression of PD-1 and Lag3 in IL-2^{lo} cultures, as well as, PD-1, Lag3 and Tim3 in IL-2_{hi} cultures (Fig 1B-E and fig S1B, S2A, table S1). Depletion of Menin (*Men1*), a key component of Mll1 and Mll2 (*Kmt2b*) -COMPASS-like complexes (*40*, *41*) exhibited similar effects (Fig 1B and fig S1B). In addition, suppression of the catalytic acetyltransferase MOZ (Myst3/ *Kat6a*), which associates with Mll1-COMPASS-like complexes, and its paralog MORF (Myst4/*Kat6b*) (*42*) also increased both PD-1 and Lag3 expression (Fig 1B and fig S1B, table S1). However, depletion of Mll2, the closest paralog of Mll1 (*39*), exhibited distinct effects (Fig 1B-D, fig S1B and fig S2A, table S1), which implies that Mll1 and Mll2 each have specific functions in CD8 T cells, analogous to their distinct requirements in other cell types (*43*). Transduction of single-guide RNAs (sgRNAs) specific for Mll1/*Kmt2a* into P14 Cas9-transgenic CD8 T cells also caused upregulation of PD-1 and Tim3 (fig S2B). Immunoblotting confirmed the on-target activity of all *Kmt2a*-specific shRNAmirs and sgRNA/Cas9-mediated disruption of *Kmt2a* (fig S3A). Thus, an Mll1-specific COMPASS-like complex might be required for controlling co-inhibitory receptor expression during TCR activation.

In the second screen, Mll1 RNAi-effects were also in the top 15% of CRFs whose depletion caused upregulation of both PD-1 and Lag3, and that impaired Id3-GFP expression (Fig 1B and fig S1B). In this setting, depletion of Mll3 (*Kmt2c*), Mll4 (*Kmt2d*), Setd1a (*Setd1a*), or Setdb1 (*Setdb1*) also impaired upregulation of *Id3*-GFP (Fig 1B, 1D, and fig S1B, table S1), suggesting that multiple Mll-COMPASS-like or Set1-COMPASS complex activities might concertedly or redundantly promote *Id3* expression during initial TCR stimulation. Additionally, depletion of Mll1 in P14 cells encoding GFP in the *Tcf7* locus ($P14^{Tcf7\text{-}GFP}$) impaired *Tcf7*-GFP expression compared to control-transduced cells (fig S3B). As expression of *Tcf7* correlates with and promotes development of cells that express Id3 (*36*, *44*), the impaired Id3 expression in the absence of Mll1 could involve reduced Tcf1 expression. Notably, Mll1-deficient cells were not generically defective, because depletion of Mll1 did not impair cell division history or overall accumulation during the first week of cell culture, or the ability to express key cytokines that are induced by T_{EFF} and T_{MEM} cells upon TCR-like re-stimulation (fig S3C-D). Thus, Mll1 is required during TCR stimulation of naive CD8 T cells *in vitro* to activate Id3 expression and to restrain expression of PD-1, Lag3 and Tim3.

Consistent with the phenotypic effects of Mll1-deficiency after TCR stimulation *in vitro*, analysis of previously published *ex vivo* gene expression data indicated *Kmt2a* expression was highest in naive cells and after day 8 post infection (pi) and in long-lived T_{MEM} cells following intracellular bacterial infection (*45*), and clustered with expression of the T_{MEM}- and T_{SCM}-associated genes *Tcf7* and *Il7r* (Fig 1F, *left*). *Kmt2a* expression was also highest in stem-like CD8 T cells after chronic LCMV infection (*19*), and clustered with expression of *Tcf7*, *Id3*, *Slamf6* and *Cxcr5* (Fig 1F, *right*). Conversely, *Kmt2a* was less highly expressed in T_{EFF} cells isolated from the early phase of acute infection (Fig 1F, *left*), and in both T_{EFF}^{trans} and

T_{EX}^{term} cells during chronic infection, and clustered apart from *Pdcd1* (PD-1), *Havcr2* (Tim3) and *Lag3* (Lag3), which were highly expressed in these cells (Fig 1F, *right*). Thus, *Kmt2a* expression is dynamic and positively correlates with formation of the most long-lived, protective T cell subsets that develop during both acute and chronic infection.

Mll1 is essential for development of T cell states that sustain responses in tumors and during chronic viral infection

To define *in vivo* requirements of Mll1, the effects of its depletion in CD8 T cells responding to engineered solid tumors expressing the GP_{33-41} epitope of LCMV (GP33) were examined in mice. P14 TCR transgenic CD8 T cells recognize GP33 and were transduced with shRNAmirs specific for Mll1 (shMll1) or negative control mRNAs (*Cd4* or *Cd19*) that are not expressed in CD8 T cells (shCon), and were co-transferred into wild type mice engrafted with B16 melanoma or E0771 triple negative breast tumors expressing GP33 fused to GFP ($B16^{GP33}$ or $E0771^{GP33}$), and their parental controls expressing GFP-only ($B16^{GFP}$ or $E0771^{GFP}$) (fig S4A). In these models, P14 cells accumulated systemically post adoptive cell transfer (pACT), but preferentially expanded and upregulated PD-1 in GP33-GFP expressing tumors, compared to the spleen or parental GFP-expressing tumors (fig S4B and fig S4C). Thus, the phenotypes of transferred P14 cells *in vivo* were induced specifically by antigen display in the tumor. Compared to shCon-transduced P14 cells in $E0771^{GP33}$ and $B16^{GP33}$ tumors, shMll1-transduced P14 cells formed significantly greater fractions of PD-1^{hi} $Tim3^{hi}$ cells (Fig 1G, p=0.0105; fig S3D, p=0.0081), and those responding to $E0771^{GP33}$ tumors exhibited higher PD-1 expression among gated $Tim3^{hi}$ cells (Fig 1G p=0.0004, fig S4E), and initially accumulated as well as, or better, than shCon-transduced cells by day 3 pACT (fig S4F). Notably, shMll1-transduced P14 cells initially delayed $E0771^{GP33+}$ tumor growth compared to transfer of shCon-transduced P14 cells, but the tumors ultimately regressed analogous to recipients of shCon-transduced P14 cells (fig S4G). Thus, Mll1-deficient cells preferentially adopted T_{EFF} cell-like states and were transiently functional in the tumor microenvironment, indicating they were not generically defective, but could not sustain tumor control.

Tumor-specific CD8 T cells that are $Tcf1^{hi}$ $Slamf6^{hi}$ and $Tim3^{lo}$ normally define a progenitor cell population with T_{SCM}-like properties that sustains the T cell response in tumors (*27*). However, shMll1-transduced $P14^{Tcf7\text{-}GFP}$ donor cells in $E0771^{GP33+}$ tumors expressed less *Tcf7*-GFP overall on day 3 pACT (fig S4H, p=0.0732), even those that were $Tim3^{lo}$ (fig S4H, p=0.0212), compared to control-transduced $P14^{Tcf7\text{-}GFP}$ cells. By day 8 pACT, shMll1-transduced cells generated significantly smaller fractions and numbers of $Slamf6^{hi}$ $Tim3^{lo}$ cells , compared to shCon-transduced cells (Fig 1H, p<0.0001). These results indicate that Mll1 is necessary for the early formation and maintenance of progenitor T_{SCM}-like cells and the persistence of responding CD8 T cells in the tumor microenvironment.

The tumor microenvironment could differentially affect the development of Mll1-deficient cells. Therefore, Mll1-depleted P14 cells were analyzed after transfer into wildtype hosts followed by infection with LCMV Clone 13 ($LCMV_{Cl13}$), which causes chronic viremia (*46*). Very early after infection, activated cells develop into $Tcf7^{hi}$ $Id3^{hi}$ $Tim3^{lo}$ exhausted cell precursor and $Tcf7^{lo}$ $Id3^{lo}$ $Tim3^{hi}$ effector cell precursor populations (*36*), that ultimately establish a continuum of cell states termed T_{EX}^{prog}, transitory effector/exhausted intermediate (T_{EX}^{trans}/T_{EX}^{int}) and terminally exhausted (T_{EX}^{term}) cells as the infection becomes chronic (*24-26*). The CRFs that initiate this pattern early during infection are unknown. On day 5 post infection (pi), both shCon-transduced and shMll1-transduced P14 cells equivalently polarized into populations of *Tcf7*-GFP^{hi} $Tim3^{lo}$ (T_{EX}-precursor) and *Tcf7*-GFP^{lo} $Tim3^{hi}$ (T_{EFF}-precursor) cells (Fig 1I, *top*). Notably, shCon-transduced T_{EX} precursors were comprised of equivalent fractions of $Slamf6^{hi}$ $CX3CR1^{lo}$ and $Slamf6^{hi}$ $CX3CR1^{hi}$ cells (Fig 1I, *top*), suggesting T_{EX} precursors manifested roughly equal bias toward

future T_{EX}^{prog} (CX3CR1^{lo}) and T_{EX}^{trans}/T_{EX}^{int} (CX3CR1^{hi}) states at this time. In contrast, shMll1-transduced *Tcf7*-GFP^{hi} Tim3^{lo} cells were predominantly Slamf6$^{int/lo}$ CX3CR1^{hi}, indicating Mll1-deficiency skewed development toward the T_{EX}^{trans}/T_{EX}^{int} state (Fig 1I, *bottom* p=0.0392). This suggests Mll1 is necessary to initially form or stabilize precursors that typically develop into T_{EX}^{prog}-like cells. Supporting this conclusion, by day 15 pi, the overall number and fraction of shMll1-transduced P14 cells among total CD8^{+} cells accumulated less and were not sustained compared to shCon-transduced cells (fig S5A). In addition, shMll1-transduced cells formed reduced fractions of *Tcf7*-GFP^{hi} Tim3^{lo} cells compared to shCon-transduced cells (Fig 1J, *top*, p=0.0571), and fewer shMll1-transduced cells that were *Tcf7*-GFP^{hi} were also CD69^{hi} compared to shCon-transduced cells at this time (Fig 1J, *bottom* p=0.0004). Thus, Mll1-deficient cells form fewer *Tcf7*-GFP^{hi} cells that develop a phenotype corresponding to *bona fide* T_{EX}^{prog1} cells (*26*).

Although Mll1-deficient cells expressed much less Slamf6 overall on day 15 pi (fig S5B), suggesting they were more effector-like, shMll-transduced cells formed smaller fractions of *Tcf7*-GFP^{lo} Tim3^{hi} cells compared to shCon-transduced cells (Fig 1J, p = 0.0001), and these were uniformly CX3CR1^{hi} (fig S5C, p=0.0230), which is atypical of canonical T_{EX}^{trans}-like cells (*26*). In addition, whereas most Slamf6$^{int/lo}$ shCon-transduced cells were CD69^{hi}, a characteristic of T_{EX}^{term} cells (*26*), most Slamf6$^{int/lo}$ shMll1-transduced cells were CD69^{lo} (fig S5B, p =0.0052). These results indicate that cells lacking Mll1 develop into non-canonical effector-like states, which do not efficiently mature into the fully exhausted phenotype during chronic infection.

Mll1 is essential for establishing the normal pattern of circulating T_{MEM} cells during acute viral infection

Strong or persistent TCR stimulation increases development of T_{EX} precursors during chronic infection (*36*) and could exacerbate or modify defects in Mll1-deficient cells. To examine if Mll1 was important for the formation of protective T_{MEM} cells, which normally develop when infections resolve rapidly and antigen is completely cleared (*11, 47*), naive shCon-transduced and shMll1-transduced P14 CD8 T cells were co-transferred to wildtype host mice subjected to LCMV Armstrong ($LCMV_{Arm}$) infection, which acutely resolves (*46*). In this setting, Mll1-deficient cells formed 2-4x fewer T_{EFF} cells at the normal peak of the response compared to control cells (Fig 2A), but subsequently decreased more sharply than control cells afterward, and formed ~10-fold fewer total T_{MEM} cells (Fig 2A).

The T_{EFF} cell population becomes heterogeneous before acute infections resolve, and only some T_{EFF} cells develop into precursors of T_{MEM} cells (*3, 12, 36, 48-51*), but how this heterogeneity is initially established is still unclear. Analysis of P14 cells labelled with cell trace violet (CTV) showed that Mll1-deficient cells initially accumulated but underwent fewer cell divisions, less efficiently sustained high *Tcf7*-GFP expression (Fig 2B *left/middle*, p =0.0286) and expressed less CD25 compared to control-transduced cells on day 3 pi (Fig 2B *right*, p= 0.0069). This indicated that the typical inverse relationship between CD25 and Tcf7 expression did not polarize in the absence of Mll1 (*16*). Furthermore, compared to shCon-transduced P14 cells on days 5 and 15 pi, those transduced with shMll1 developed reduced fractions of CD27^{hi} CX3CR1$^{lo/int}$ and CD27^{int} CX3CR1^{int} cells, which normally harbor precursors of central memory (T_{CM}) cells (Fig 2C, p<0.0001,p=0.0022) (*52*), were mainly KLRG1^{hi} (Fig S6A, p<0.0001) and comprised a much larger fraction of CD27^{lo} CX3CR1^{hi} cells (Fig 2C, p<0.0001), which normally comprise precursors of T_{EM} cells and terminally differentiated effector (TE) cells (*51-53*). Although shMll1-transduced cells were as abundant as shCon-transduced P14 cells in the spleen on day 5 pi (Fig 2A), they incorporated less EdU, indicating they were proliferating less at this time (Fig S6B, top, p=0.0004). By day 8 pi, shMll1-transduced P14 cells formed lower frequencies of KLRG1^{lo} CD127^{hi} classical memory precursor (MP) cells (*51*) compared to shCon-transduced cells, and were virtually devoid of KLRG1^{lo} CD127^{lo} "early effector" (EE) cells (Fig 2D, p=0.0078, p<0.0001). These phenotypes were confirmed using P14-Cas9 transgenic cells transduced with Mll1-specific single-guide RNAs (sgMll1, fig S6C, p=0.2507, p=0.0216). In addition,

KLRG1^{hi} shMll1-transduced P14 cells incorporated less EdU on day 8 pi (Fig S6D, p=0.0146), indicating they were less proliferative than shCon transduced KLRG1^{hi} cells at the peak of the response. Altogether these results suggest Mll1-deficiency prevented initial formation of conventional precursors of recirculating T_{CM} and T_{EM} cells, and promoted terminal differentiation.

T_{EFF} cells that most highly express *Tcf7* at the peak response to acute viral infection appear to be T_{SCM} precursors that form T_{CM} cells (*12*). On day 15 pi, all phenotypic subsets of shMll1-transduced P14$^{Tcf7\text{-}GFP}$ cells expressed significantly less *Tcf7*-GFP compared to shCon-transduced cells (Fig 2E). Over time, the frequencies of shMll1-transduced P14 cells exhibiting a terminal T_{EM} (t-T_{EM}) phenotype (CD62L^{lo} CD127^{lo}) decreased (Fig 2F, *right*), those exhibiting a T_{EM} (CD62L^{lo} CD127^{hi}) phenotype were mainly constant (Fig 2F, *middle*), and those with a central memory (T_{CM}) phenotype (CD62L^{hi} CD127^{hi}) increased (Fig 2F, *left*). However, the numbers of each phenotypic subset decreased strongly (fig S6E), as might be expected from their reduced *Tcf7*-GFP expression (*17*). We considered that the preferential persistence of shMll1-transduced cells with a T_{CM}-phenotype was because CD27^{hi} T_{EFF} cells retained some *Tcf7*-GFP expression, suggesting they could have developed into functional T_{CM} cells. To test this, CD62L^{hi} and CD62L^{lo} shCon-transduced and shMll1-transduced P14 cells were isolated 90 days after primary $LCMV_{Arm}$ infection, and 1:1 mixtures of shCon-transduced and shMll1-transduced cells that were either CD62L^{hi} or CD62L^{lo} were co-transferred to new naive hosts, and were then infected with *Listeria monocytogenes*-GP33 (LM_{GP33}) to mimic a secondary infection (Fig 2G and fig S6F). On day 5 after LM_{GP33} infection, CD62L^{hi} donor P14 cells that were shMll1-transduced accumulated 5-10 fold less than shCon-transduced cells and formed a reduced fraction of secondary CD27^{hi} CX3CR1^{lo} T_{CM} precursors (Fig 2G $p<0.0001$). In contrast, the accumulation of both shMll1-transduced and shCon-transduced CD62L^{lo} donor cells was similar, but much less than the CD62L^{hi} transferred cells (Fig 2G and fig S6F), as expected of T_{EM} cells (*54*). Thus, Mll1 is essential for establishing Tcf7^{hi} memory precursors during the effector response and for forming *bona fide* CD62L^{hi} T_{CM} cells in the memory phase.

Mll1 coordinately induces T_{MEM} gene expression and represses TE gene expression

To examine how Mll1 controls gene expression before T_{CM} cells definitively form, RNA-seq was used to analyze shMll1-transduced or shCon-transduced P14 T_{EFF} cells in the spleen that were either KLRG1^{lo} or KLRG1^{hi} 5 days after $LCMV_{Arm}$ infection (fig S7A, and table S2). Analysis of shCon-transduced cells indicated KLRG1^{lo} cells more strongly expressed signatures characteristic of stem or progenitor stem-like cells, whereas KLRG1^{hi} cells more strongly expressed signatures of day 8 KLRG1^{lo} CD127^{lo} early effector (EE) and TE cells (fig S7B). TCR-induced gene expression (Fig 3A, *TCR dependent*) and the *Tcf7*^{hi} effector cell signature (*12*) were less strongly upregulated by shMll1-transduced cells compared to shCon-transduced cells in both KLRG1^{lo} and KLRG1^{hi} populations (Fig 3A, *Day 8 $LCMV_{Arm}$*). The genes *Bcl6, Id3, Jund* and *Il6ra* in KLRG1^{lo} cells are normally more highly expressed in MP cells then TE(*55*), but were less highly expressed in shMll1-transduced KLRG1^{lo} cells compared to shCon-transduced (fig S7C, *left*, table S2). In addition, gene expression driven by Tcf1 and Tox, which is positively associated with progenitor T_{SCM}-like cells, was less highly expressed in shMll1-transduced KLRG1^{hi} cells, compared to shCon-transduced cells (Fig 3A, *TCR dependent*). Reciprocally, shMll1-transduced cells overexpressed the signature of TE cells in both KLRG1^{lo} and KLRG1^{hi} populations (Fig 3A, *Day 8 $LCMV_{Arm}$*), including the TE-signature genes *Zeb2, Bhlhe40, Ccl5* and *Cx3cr1*, compared to shCon-transduced cells and they also reactivated genes that are normally expressed in naive cells (Fig 3A, *TCR dependent*, fig S7C, *right* and table S2). Thus, Mll1 is necessary to activate expression of factors in both KLRG1^{lo} and KLRG1^{hi} cells that normally promote formation of long-lived T_{MEM} cells, and to repress aberrant co-expression of genes expressed by naive cells and TE cells.

Mll1 promotes transcription of dynamic genes that drive development of nascent T_{SCM} precursors

Tcf7^{hi} T_{EFF} cells might comprise T_{SCM} cells that bypass full T_{EFF} cell differentiation during acute infection (*12*, *16*), but the transcriptional control that specifies their early formation is still unclear. We anticipated that the effect of Mll1-deficiency on early developmental trajectories might clarify this process, and therefore used single-cell RNA-sequencing (scRNA-seq) to analyze shCon-transduced and shMll1-transduced P14 cells 5 days after $LCMV_{Arm}$ infection in the context of cells isolated on days 3 and 8 pi that derived from separate transfers of small numbers of wildtype naive P14 cells. Cells from all time points separated into 13 Leiden clusters (Fig 3B, *top*), and were numbered according to increasing latent time to define a potential developmental order (fig S8A). In the unsupervised arrangement, transduced cells from day 5 pi were concentrated in clusters located between clusters that mainly comprised cells from days 3 and 8 pi, consistent with their development in actual time (Fig 3B, *bottom*). The enrichment of known gene expression signatures aided defining the biological nature of cells in each cluster (Fig 3C). Cells transduced with shCon or shMll1 contributed to the clusters differentially (Fig 3D), and exhibited distinct RNA velocity-derived transition probabilities (Fig 3E-F and fig S8B), indicating they propagated through the trajectory differently.

Cluster T1 comprised TCR-activated intermediates enriched with the signature of T_{CM} cells (Fig 3C) and exhibited transition potential into clusters T2 and T3 (fig. S8B). Cluster T2 comprised a small number of cells from day 3 pi that strongly repressed the *Tcf7*^{hi}-effector cell signature (Fig 3C). In contrast, cluster T3 comprised a larger number of shCon-transduced cells from day 5 pi that upregulated the signatures of *Tcf7*^{hi}-effector and T_{prog} cells (Fig 3C). Cells from cluster T3 branched into cluster T5 (fig S8B), an activated and unbiased T_{EFF}-like state (Fig 3C), and into cluster T6 (fig S8B), a state positively enriched with signatures of both KLRG1^{hi} CD127^{hi} double positive (DP) effector cells, and tissue-resident memory (T_{RM}) cells (Fig 3C). This suggests most activated cells initially express Tcf1-driven gene expression before effector cell specification occurs, consistent with prior studies (*49*). However, shMll1-transduced cells were virtually absent from cluster T3, and significantly fewer contributed to clusters T5 and T6 compared to shCon-transduced cells (Fig 3D). Residual shMll1-transduced cells from cluster T3 were negatively enriched Tcf1 and Tox-promoted gene expression and the signatures of *Tcf7*^{hi}-effector and T_{prog} cells compared to shCon-transduced cells (fig S8C), and lacked transition potential into either clusters T5 or T6 (fig S8B). Thus, Mll1 was required for the development or stability of activated cell states that sustain T_{SCM}-related gene expression.

Mll1 governed the transition potential of cells in cluster T5, which normally diverged into cell states that either sustained and upregulated the signature of *Tcf7*^{hi} effector cells, or that downregulated this signature and acquired effector-like signatures. Control-transduced P14 cells in cluster T5 had transition potential into clusters T7, T8, and T9, whereas shMll1-transduced T5 cells exhibited transition potentials into clusters T6 and T9 (Fig 3E and fig S8B). Thus, Mll1 normally promotes transition into clusters T7 and T8. Con-transduced cells in clusters T7 and T8 maintained the expression of both *Tcf7*^{hi} effector and T_{prog} cell signatures (Fig 3C, *Day 8 $LCMV_{Arm}$*), upregulated genes expressed by memory and naive cells (Fig 3C, *naive & memory*, *IV*) and repressed gene expression of acutely activated cells (Fig 3C, *early activation genes*, *III*), whereas those in cluster T9 less strongly expressed the *Tcf7*^{hi} effector and T_{prog} signatures compared to clusters T7 and T8, maintained expression of early activation genes (Fig 3C, *early activation genes*, *III*), and upregulated the signatures of both DP effector cells and T_{RM} cells (Fig 3C, *Day 8 and Day 30 $LCMV_{Arm}$* signatures). Conversely, shMll1-transduced cells in all three of these clusters less highly expressed genes normally induced by Tcf1 and Tox and overexpressed gene expression promoted by the TFs T-bet (*Tbx21*) and Blimp1 (*Prdm1*) (fig S8C-D). Thus, Mll1-deficient T5 cells did not normally establish T_{SCM}-related gene expression, were effector-cell biased and preferentially diverged into effector-like states, suggesting this was a proximal defect of Mll1 deficiency.

To define how gene expression regulated the developmental potential of cells in cluster T5, the genes whose transcriptional behavior was most dynamic between clusters (driver genes) were extracted from shCon-transduced and shMll1-transduced cells. Driver genes explain the derived transition potentials of cells (*56*) in the trajectory and were substantially distinct in shCon-transduced and shMll1-transduced cells (table S4). The drivers in shCon-transduced cells identified from the entire trajectory (Fig S8E), and

those specifically extracted from clusters T5 and T9 (Fig. 3F) were significantly enriched among genes that were more highly expressed in shCon-transduced cells, suggesting that their normal dynamics in the trajectory involved positive regulation by Mll1. In addition, driver genes specific to shCon-transduced cells from clusters T5 and T9, or common to both shCon-transduced and shMll1-transduced cells from both clusters (Fig S8F), were more highly expressed in shCon-transduced cells of cluster T5 compared to T9 (fig S8G, p=0.0002), whereas those exclusive to shMlll-transduced cells were more highly expressed in shCon-transduced cells from cluster T9 than in cluster T5 (fig S8G, p=0.0077). Together, these results suggest that Mll1 is required to activate driver genes whose dynamics explain early developmental transitions and to prevent activation of alternative driver genes that explain transition into later states. TCR stimulation was likely to positively regulate the dynamics of driver genes in cluster T5, because genes that are transiently induced 24 and 48 hours after acute infection were more highly expressed in cluster T5 cells (Fig 3C, *early activation II*, and *III*). In addition, nascent transcription of driver genes in shCon-transduced cells from cluster T5 were strongly regulated in naive CD8 T cells upon TCR and co-stimulation (Fig 3G). Thus, the transcriptional dynamics of genes which account for early transition potentials appear to be governed by TCR-signals and positively regulated by Mll1.

Cluster T11 appeared to be a distinct T_{SCM} precursor state because it was most strongly enriched with the signatures of *Tcf7*^{hi} effector and T_{prog} cells compared to all clusters in the trajectory, and had upregulated both naive and memory cell-associated gene expression including the T_{CM} cell specific signature (Fig 3C). Cluster T11 cells mainly derived from transduced cells on day 5 pi and bridged development into cell states from day 8 pi that first repressed the Tcf7^{hi}-effector and T_{prog} signatures (cluster T12) and then transitioned into cluster T13 which activated TE cell gene expression (Fig 3E and fig S8B). Thus, T_{EFF} cell populations found in the spleen on day 8 pi developed directly from a distinct T_{SCM}-like precursors on day 5 pi. Compared to shCon-transduced cells in cluster T11, gene expression in shMll1-transduced cells was negatively enriched with signatures of *Tcf7*^{hi} effector, T_{prog} and mature T_{CM} cells, but was positively enriched with signatures of TE and T_{EM} cells (fig S8C). Differential expression demonstrated that shMll1-transduced T11 cells expressed significantly less of the *Tcf7*^{hi} effector cell signature genes *Tcf7*, *Tox*, *Aff3*, *Bcl2*, *Ltb*, *Slamf6* and *Ctla2a* and significantly more of the TE cell signature genes *Klrg1*, *Gzma*, *Ccl5*, and *Cd48* (Fig 3H, p=0.0002 and p=0.0046 respectively). In contrast, there was no bias in the number of *Tcf7*^{lo} effector cell signature genes that were differentially expressed in shCon-transduced cells compared to shMll1-transduced cells, indicating that the reciprocal effects of Mll1-deficiency on *Tcf7*^{hi} effector and TE cell gene expression were specific (p=0.1522). These results indicate Mll1 stabilizes an early T_{SCM} precursor state and prevents premature activation of TE cell gene expression, which explains the altered frequency distributions of TE and MP cells that develop from shMll1-transduced cells on day 8 pi (Fig 2D).

Mll1 pioneers widespread and T_{MEM}-specific H3K4me3 deposition at TSSs during TCR stimulation

The mechanics that program enhanced transcriptional competence in T_{MEM} cells compared to naive cells are still unknown. Histone H3 lysine 4 tri-methylation (H3K4me3) deposition near transcription start sites (TSSs) defines poised and active promoters (*57*), and may positively regulate transcriptional elongation (*58*). Many genes lacking H3K4me3 in naive CD8 T cells acquire this modification in mature T_{EFF} and T_{MEM} cells (*31, 59*), suggesting it is a key chromatin regulatory step that differentiates T_{MEM} cells from their naive ancestors. Although Mll1 is the archetype H3K4-trimethylase (*60, 61*), its disruption in mammals has only demonstrated reductions in H3K4me3 at limited number of genes and other COMPASS-family methyltransferases are thought to establish and maintain the majority of H3K4me3 (*43, 62, 63*). However, we found that during TCR stimulation the relative abundance of H3K4me3, and RNA Polymerase II (Pol II) hyperphosphorylated on serine-5 (Ser5-P) or serine-2 (Ser2-P) C-terminal domain (CTD) residues (fig S9A) increased in conjunction with expression of the catalytic component of MLL-COMPASS-like complexes (Mll1-C), suggesting that Mll1 could promote transcriptional reprogramming during initial naive cell activation.

ChIP-seq analysis demonstrated that regions of H3K4me3 deposition ("peaks") in naive and TCR-stimulated cells overlapped extensively with those present in *ex vivo* T_{MEM} (KLRG1^{lo} CD127^{hi}) cells (*31*),

indicating that naive and antigen-experienced CD8 T cells share an extensive core H3K4me3 landscape (*31, 59*) (fig S9B). In addition, TCR stimulation remodeled the naive cell landscape by transiently reducing H3K4me3 at some peaks relative to naive cells and progressively increasing *de novo* H3K4me3 peaks, which increasingly overlapped those present specifically in *ex vivo* T_{MEM} cells (Fig 4A, fig S9B). Notably, approximately 20% of all peaks that exhibited significantly greater H3K4me3 in T_{MEM} cells relative to naive cells were induced within the first 72 hours of TCR-stimulation (fig S9B). Thus, a substantial fraction of the T_{MEM} cell-specific H3K4me3 landscape is established during initial TCR stimulation, and is potentially maintained "epigenetically" as some activated cells develop into T_{MEM} cells.

Genes that acquired H3K4me3 during TCR stimulation were more highly expressed in TCR-activated cells, and in both Tcf7^{hi} and Tcf7^{lo} T_{EFF} cells relative to naive cells, as well as in mature Tcf7^{hi} memory cells and T_{CM} cells, relative to t-T_{EM} cells (fig S9C-D). Thus, initial TCR stimulation induced H3K4me3 deposition at genes that become expressed in both T_{EFF} and long-lived T_{MEM} cells. Acute depletion of Mll1 during TCR stimulation significantly reduced H3K4me3 deposition at more than half (~8,000 peaks) of all peaks identified in TCR activated cells (~15,000 total peaks) (Fig 4B). This included ~70%, and 49% of all *de novo* H3K4me3 peaks induced 24, or 72 hours after TCR stimulation, respectively, and ~70% of all H3K4me3 peaks that are normally upregulated in mature T_{MEM} cells that comprised a mixture of T_{CM} and T_{EM} cells (KLRG1^{lo} CD127^{hi} D60, LM_{Ova} (*31*)) compared to naive cells (Fig 4C-D). Within activation-dependent H3K4me3 peaks, regions dependent on Mll1 for H3K4me3 during TCR stimulation were positively enriched among genes that were more highly expressed in TCR stimulated cells (Fig 4E, *left*). In addition, Mll1-dependent H3K4me3 regions induced 24 hours after TCR stimulation were specifically enriched in genes that were more highly expressed in T_{CM} cells (CD62L^{hi} CD127^{hi}) relative to either T_{EM} (CD62L^{lo} CD127^{hi}) or t-T_{EM} cells (CD62L^{lo} CD127^{lo}) analyzed 30 days after $LCMV_{Arm}$ infection (Fig 4E, *right*)(*64*); and those from T_{MEM} cells were positively enriched in genes more highly expressed in T_{CM} cells relative to t-T_{EM} cells (Fig 4E, *bottom right*). Thus, Mll1 was specifically required during initial TCR stimulation for H3K4me3 deposition in regions that define a large fraction of the T_{MEM} cell chromatin landscape, especially those specific to T_{CM} cells.

Mll1 facilitates RNA Polymerase II elongation of dynamic genes during TCR stimulation

As expected, transcription positively correlated with H3K4me3 deposition in both naive and TCR-stimulated cells (Fig S9E). TCR stimulation increased H3K4me3 deposition and transcription of genes that were upregulated during the first 48 hours of infection, which included signature genes expressed in both Tcf7^{hi} and Tcf7^{lo} effector cells (Fig S9E, *top*). However, many genes that acquired H3K4me3 upon TCR stimulation did not immediately induce transcription, suggesting their full transactivation might depend on additional signals (Fig S9E). These predominantly comprised genes expressed in naive cells (blue) or genes that are upregulated in T_{EFF} or T_{MEM} cells at late times after infection (Fig S9E, *bottom*). Thus, TCR-induced H3K4me3 deposition correlated with immediate transcriptional activation, and established the potential for future transcriptional activation of T_{MEM}-associated genes.

Analysis of total Pol II occupancy by ChIP-seq indicated that primary TCR stimulation induced widespread transcriptional pausing at genes that underwent H3K4me3 installation. Genes induced transcriptionally by TCR stimulation exhibited increased promoter and gene body-associated Pol II occupancy, compared to naive cells (Fig 4F and fig S10A). However, Pol II density at promoters increased more than in gene bodies, suggesting elongation of recruited Pol II became limiting upon TCR stimulation (fig S10A). Accordingly, Pol II pausing indices increased in genes that acquired H3K4me3 upon TCR stimulation (Fig 4F, fig S10B, table S5), in those whose transcriptional dynamics explained transition probabilities of cells in the trajectory analysis (Fig 4G, *middle*, table S5), and in those with greater H3K4me3 specifically in T_{MEM} (LM_{Ova} D60) cells compared to naive cells (Fig 4G, *right*, fig S10A, table S5). In contrast, genes marked with H3K4me3 specifically in naive cells exhibited a modest increase in their pausing indices in naive cells compared to TCR stimulated cells (Fig 4G, *left*, table S5). Thus, primary TCR stimulation induces H3K4me3 installation and Pol II pausing specifically in genes that establish the formation of T_{EFF} (LM_{Ova} D8) and T_{MEM} cells and that were Mll1-controlled. These results suggest that increased transcription of these genes is regulated by promoting release of paused Pol II (elongation).

To determine how Mll1 governed transcription, its binding was mapped in activated CD8 T cells using ChIP-exo5.0 (*65*). Mll1 primarily bound to the TSSs of active genes marked with H3K4me3, rather than promoter-distal hyper-accessible ATAC-seq regions marked with H3K4me1 (fig S10C). The summit of Mll1 occupancy localized 92bp downstream of TSSs (Fig 4H, *teal*) coincident with the summit of paused Pol II (Fig 4H, +90bp, *rose*), which was immediately upstream of an MNase-protected region corresponding to +1 nucleosomes (Fig 4H, *black*) and the summit of H3K4me3 density (Fig 4H, +230bp, *gold*). Mll1 signal was not enriched upstream of the TSS (Fig 4H, fig S10C). Thus, Mll1 was most likely recruited to paused Pol II near +1 nucleosomes after TCR activation. Depletion of Mll1 during TCR stimulation further increased promoter Pol II occupancy in the pause region (Fig 4I), resulting in increased Pol II pausing indices of dynamic genes (Fig 4J, *top*, table S5), and genes that required Mll1 for TCR-stimulation dependent H3K4me3 deposition (Fig 4J, *bottom* and 4K, table S5). Consistent with these results, depletion of Mll1 in TCR stimulated cells globally decreased both initiating (Ser5-P) and elongating (Ser2-P) forms of Pol II (Fig 4L)(*66*), suggesting Mll1 promotes transcription initiation and elongation. In line with these observations, shMll1-transduced cells exhibited a global decrease in molecule counts per cell in the scRNA-seq data (fig S10D), suggesting they manifested a broad defect in transcriptional activation in TCR stimulated cells *in vivo*. Thus, Mll1 most likely promotes efficient Pol II elongation upon TCR stimulation. Notably, Mll1-dependent deposition of H3K4me3 occurred immediately downstream of the Mll1 binding location (Fig 4M), suggesting that it might occur after Mll1-facilitated Pol II elongation events. Thus, Mll1 appears to have an early role in establishing H3K4me3 in T_{MEM}-associated genes during the initial activation of naive CD8 T cells.

Conclusion:

Chromatin accessibility that develops in human CD8 T_{EFF} cells during the first week of live viral vaccination persists in slowly dividing T_{MEM} cells for nearly a decade (*11*), but the CRFs and transcriptional mechanics that establish and maintain these states are ill-defined. Our results demonstrate that Mll1 is essential for widespread H3K4me3 deposition during primary TCR stimulation, activation of T_{SCM} cell-associated gene expression and formation or stability of cells with T_{SCM}-like phenotypes and functions during infections and tumors *in vivo*. In addition, we show that TCR stimulation and Mll1 regulate Pol II pausing in genes whose transcriptional dynamics *in vivo* drive early heterogeneity of activated CD8 T cell states during viral infection. These results are consistent with a model in which Mll1 configures Pol II at promoters for responsiveness to signals that govern Pol II pause release and transcriptional elongation to both specify early T_{EFF} cell developmental trajectories and to enable long-term capacitance of transcriptional activity in T_{MEM} cells. Notably, deposition of H3K4me3 at the 5' ends of genes is known to occur as Set1-methyltransferases traffic with elongating polymerases (*67*). Our analyses indicate that Mll1 could traffic with Pol II to directly deposit H3K4me3, or potentiate the action of additional methyltransferases by facilitating modification and release of paused Pol II. In either model, Mll1 pioneers early H3K4me3 deposition during TCR stimulation that initially establishes the chromatin architecture of transcriptionally poised and active genes that define long-lived T_{MEM} cells.

Acknowledgments:
We would like to thank the Karbstein, Solt, and Sundrud labs for reagents and productive conversations, the Nettles lab for helping develop the E0771 model, and Dapeng Wang for performing initial MNase experiments. We would also like to thank the Flow Cytometry, the Genetic Perturbation Screening, and Genomics Cores at the Wertheim UF Scripps Institute for resources and services.

Funding:
National Institutes of Health grant: P01AI145815 (MEP,AWG, and SC)
National Institutes of Health grant: U19AI109976 (MEP,AWG, and SC)
National Institutes of Health grant: R01AI095634 (MEP)
National Institutes of Health grant: F31CA232380 (AJG)

Author contributions:
Conceptualization: AJG, MAF, JJM, TV, HD, and MEP
Data curation: AJG, MAF, JJM, TV, and HD
Formal analysis: AJG, MAF, JJM, TV, HD, SDN
Funding acquisition: AJG, SC, AWG, and MEP
Investigation: AJG, MAF, JJM, HD, CT, SDN, DSA, SMT, and JK
Methodology: AJG, MAF, JJM, SB, SMT, and MEP
Project administration: AJG and MEP
Resources: SB, SC, AWG, and MEP
Software: AJG, TV, HD, and SDN
Supervision: SC, AWG, and MEP
Validation: AJG, MAF, JJM, and TV
Visualization: AJG, MAF, JJM, TV, and MEP
Writing original draft: AJG and MEP
Writing review and editing: All authors

Figures

Fig 1. Identification of Mll1 as an essential regulator of progenitor T_{SCM}-like cell formation

(**A**) Arrayed RNA interference screening layout. (**B**) The average RNAi effect resulting from suppression of individual CRFs on expression of *Id3*-GFP (left, $d3^{TCR}$) and PD-1 (right, IL-2^{hi}) in each screen. Dashed line indicates top and bottom 15th percentile. (**C**) Bar charts show the mean raw expression values (geometric mean fluorescent intensity) of *Id3*-GFP (top) and PD-1 (bottom) in response to each cognate shRNAmirs (symbols). P values were calculated using Welch's t-test. (**D**) RNAi-effects for COMPASS (blue) and BAF (red) complex subunits in each screen were clustered by Euclidean distance. (**E**) Representative flow cytometry data of individual shRNAmirs targeting a non-expressed gene (shCon, gray) or Mll1 (shMll1, blue) in each screening condition. Numbers in plots indicate geometric mean fluorescence intensity. (**F**) Heatmaps show normalized transcript counts of selected COMPASS, COMPASS-like, T_{SCM} and T_{EX} cell signature genes in purified antigen-specific CD8 T cells responding to Listeria monocytogenes-Ova (LM-Ova) (*45*), or $LCMV_{Cl13}$ (*25*). Intensity of color represents highest expression of an individual gene across columns. (**G-H**) Representative flow cytometry plots after gating on P14 $CD8^+$ T cells transduced with shRNAmirs specific for negative control genes (shCon) or Mll1 (shMll1) in $E0771^{GP33}$ tumors, and comprise concatenated data from multiple mice (n=3). Histogram overlay shows geometric mean fluorescent intensity (gMFI); gating is indicated. Bar charts summarize the means of individual mice (symbols). P values calculated via paired Student's t-test. (**I-J**) Representative flow cytometry plots after gating on adoptively co-transferred $P14^{Tcf7\text{-}GFP}$ $CD8^+$ T cells transduced with either control (shCon) or Mll1 (shMll1) specific shRNAmirs from the spleens of host mice 5 or 15 days after $LCMV_{Cl13}$ infection. Data was concatenated from multiple recipient mice (I, n=3; J, n=4). $Tcf7^{hi}$, $Tim3^{lo}$ cells (top) were gated and analyzed for Slamf6 and CD69 expression (bottom). Bar charts summarize the means of individual mice (symbols). P values calculated via Welch's t-test, except for J (top), which used the Mann-Whitney test.

Fig. 2. Mll1 is essential for development of T_{MEM} cells following acute viral infection.

P14 or $P14^{Tcf7\text{-}GFP}$ $CD8^+$ T cells transduced with either control (shCon) or Mll1 (shMll1) specific shRNAmirs were adoptively co-transferred into wildtype host mice subjected to $LCMV_{Arm}$ infection (A-F). (**A**) P14 cell accumulation. Symbols indicate normalized transduced P14 cell numbers in the spleen. Shaded plot indicates normalized percent of transduced P14 cells of all $CD8^+$ T cells. Both data present the mean of n≥3 individual mice. (**B**) Naive P14 cells were cell trace violet (CTV) labeled before transduction, and the

percent of each transduced population that underwent more than the median number of divisions by day 3 pi in the spleen is indicated in the plot (left). Histograms show the gMFI of *Tcf7*-GFP (middle) and CD25 expression (right). Numbers in plots indicate gMFI of each marker, which are summarized in bar charts as the means for all mice (symbols). Paired t-test used to compare means. Representative flow cytometry data concatenated from four recipient mice. (**C-F**) Representative flow cytometry of transduced P14 $CD8^+$ T cells in the spleen are data concatenated from 3-5 mice. Values in plots indicate frequencies, and are summarized as means in bar charts for all mice (symbols). Mice with less than 10 transduced cells (day 90 pi) were excluded from statistical analyses of cell frequencies, and the mean normalized transduced P14 cell numbers per spleen were summarized for individual mice (symbols) in (F). Paired t-test or Wilcoxon test were used to compare means. (**E**) The representative histograms analyzed expression *Tcf7*-GFP in phenotypic populations after gating on transduced $P14^{Tcf7\text{-}GFP}$ $CD8^+$ T cells. Numbers in plots indicate gMFI and are summarized for all mice (symbols). Paired t-test used for statistics. (**G**) The accumulation of donor derived $CD62L^{hi}$ or $CD62L^{lo}$ memory cells from day 90 pi that were either shCon or shMll1 transduced were mixed, adoptively transferred to naive wildtype hosts and subjected to LM^{GP33} infection. The abundance (left) and phenotype (right) of transduced P14 cells were analyzed on 5 pi in the spleen. Transduced P14 cell numbers and frequencies of phenotypic subsets were summarized for all mice (symbols) in bar charts. Paired t-tests used for statistics.

Fig 3: Mll1 promotes transcriptional dynamics that establish a nascent T_{SCM} precursor state

(**A**) RNA-seq analysis examined shCon and shMll1-transduced $KLRG1^{lo}$ and $KLRG1^{hi}$ P14 cells in the spleen 5 days after $LCMV_{Arm}$ infection. The enrichment of specific gene signatures (left) were analyzed against the Wald statistic of shMll1 vs shCon-transduced cells. (**B**) PAGA initialized force assisted analysis of the scRNA-seq data depicts Leiden clusters (top) and the cells of origin (bottom). (**C**) The specific expression of gene signatures (indicated on left) (*1, 2, 12, 45, 55, 68*) were analyzed within each Leiden cluster using Wilcoxon ranked score of the change in expression within each cluster versus all other clusters. (**D**) Cell numbers in each Leiden cluster are indicated (blue heatmap, top). Stacked bar charts indicate the frequency distribution of cells from each sample in Leiden clusters (middle), and the fraction of cells from each sample in each cluster (bottom). (**E**) RNA velocity vector fields for shCon (top) and shMll1 (bottom)-transduced cells in clusters T5-T9. The table inset indicates the intercluster transition potentials. Note distinct transition potentials from cluster T5 in shCon versus shMll1-transduced cells. (**F**) The bias in expression of dynamic genes identified in shCon-transduced cells from clusters T5 and T9, was analyzed using GSEA and the scRNA-seq data ($\log_2$ fold change, Wilcoxon rank) to compare shCon versus shMll1-transduced cells. (**G**) Purified naive CD8 T cells were stimulated with plate-bound anti-CD3 and anti-CD28 (TCR) and chromatin-associated RNA (nascent transcription) was analyzed before and after stimulation. The heatmap depicts the $\log_2$ fold-changes in expression for the top 10th percentile of dynamic genes that explained the transition potential of shCon cells in cluster T5 (i.e., not dynamic in shMlll cells), and that were also differential 48 hours after TCR stimulation (padj<=0.05), and were clustered by Euclidean distance. The expression of these genes in shMll1 versus shCon-transduced cells in the scRNA-seq data is also shown (*bottom* row). Chi-squared test for each row tests the fraction of genes that were upregulated against the fraction of genes upregulated in all genes in the given dataset. (**H**) Differential gene expression between shMll1 and shCon transduced cells in cluster T11 ($\log_2$ fold change, Wilcoxon rank) is displayed as a volcano plot. Genes highlighted in blue are significantly regulated genes within the TCF^{hi} gene set; those in red within the TE set.

Fig 4: TCR signals and Mll1 establish T_{MEM} cell-specific H3K4me3 deposition and RNA Pol II pausing

(A) Bar chart shows the number of differential H3K4me3 peaks in activated versus naive cells ($\log_2$ fold change, P <= 0.05). (**B**) H3K4me3 peaks were annotated to the nearest gene and the average $\log_2$ fold

change and false discovery rate (FDR) was calculated per gene in shCon-transduced (left) versus shMll1-transduced cells (right) 72 hours after TCR stimulation. The number of genes (grey) and those harboring T_{MEM} specific H3K4me3 peaks (dark blue dots) that were differential (FDR < 0.05) are indicated. (**C**) Stacked bar chart shows the number and fractions (white numbers) of H3K4me3 peaks that form after naive cells have been activated (red) whose H3K4me3 signal is significantly greater in shCon compared to shMll1 transduced cells 72 hours after TCR stimulation (blue bar). (**D**) Genome tracks show TCR-dependent and Mll1-dependent H3K4me3 deposition in representative genes. Coverage normalized to sequencing depth, and track heights normalized across TCR stimulated, naive and LM_{Ova} samples independently. (**E**) Bubble plot quantifies enrichment of differential gene expression (Wald statistic) from the indicated comparisons within genes harboring annotated H3K4me3 peaks that exhibited significantly increased H3K4me3 density in TCR-activated or T_{MEM} (LM_{Ova} D60) cells compared to naïve cells that were also dependent on Mll1 for H3K4me3 depostion(signatures). The bound set contains all genes bound by Mll1. (**F**) The fraction of total Pol II reads from naive cells (black) and cells activated by TCR and co-stimulation for 72 hours (red) located +/-1 kb of the TSS was calculated per base pair and plotted around the TSSs of genes induced transcriptionally by TCR signals (48 hours TCR versus naive, chromatin associated RNA-seq, P adj. < 0.05). (**G**) The ratio of normalized Pol II counts in promoters (-50bp to +300bp) to counts in gene bodies (+301 to +600 bp) (pausing index) was calculated using Pol II data from naive (black) and TCR-stimulated (72 hours, red) cells. Pausing indices were plotted as empirical cumulative distribution functions (eCDFs, P values computed with Kolmogorov Smirnov test) for genes with greater H3K4me3 in naive cells (naive H3K4me3), all dynamic genes from day 5 pi (see Fig 3G, Day 5 dynamic genes), and genes with greater H3K4me3 in T_{MEM} cells compared to naive cells (LM_{Ova} D60 H3K4me3). (**H**) ChIP-seq and MNase-seq signals centered on Mll1-bound TSSs were plotted. Coverage was scaled across samples and calculated on a per bp level. (**I**) The fraction of total Pol II reads in shCon (grey) and shMll1 (blue) cells located +/-1 kb of the TSS of genes dependent on Mll1 for H3K4me3 deposition (FDR <= 0.05) were calculated per base pair and plotted. (**J**) The pausing indices of the indicated gene sets from shCon (grey) and shMll1 (blue) are plotted as eCDFs as in (G). (**K**) The deposition of H3K4me3 and Pol II is shown for representative loci in shCon (grey) and shMll1 (blue) tracks 72 hours after primary TCR stimulation. Coverage was normalized to sequencing depth. (**L**) Naive P14, or P14 Cas9-transgenic, CD8 T cells were transduced 16 hours after initial TCR stimulation with either shRNAmir-expressing retroviruses (*top*), or sgRNA-expressing retroviruses (*bottom*), respectively. Transduced cells were purified by FACS 72 hours after stimulation, equivalent cell numbers were solubilized in RIPA buffer and the resulting pellet (*left*) and supernatant (*right*) fractions were recovered and resolved by PAGE and analyzed by immunoblotting. (**M**) Binding of Mll1 (teal) and H3K4me3 from shCon (grey) and shMll1 (blue) at Mll1 bound TSS's. Coverage was scaled to read-depth and calculated on a per bp level.

Vectors, shRNAmirs, CDNA constructs and retroviral packaging

The MSCV-based retroviral vectors MigR1, LMPd, and LsgA were used to transduce activated $CD8^+$ T cells. MigR1 encoding IRES-GFP, was used to deliver *RUNX3* (long form) CDNAs(*55*). LMPd, encoding Pgk-Ametrine1.1 or Venus was used to express shRNAmirs, whose sequence was predicted by the shERWOOD algorithm and were purchased from TRANSOMICS(*69-71*). The LsgA vector was previously described and the Chop-Chop program was used to design guides(*72*). Retroviral supernatants were generated in Platinum-E packaging cells as previously described(*69*).

Mice

C57BL/6J mice used in this paper were obtained from the Jackson Laboratory. P14 $Thy1.1^+$ mice were a gift from R. Ahmed (Emory University). $Thy1.1^+$,$Thy1.2^+$ positive mice were generated by crossing the P14 mice to wildtype BL/6J mice. The Tcf7 reporter mice were purchased from Jackson and crossed to P14 mice to create P14-Tcf7 mice (*73*).The P14 $TCRa^{-/-}$ were initially purchased from Taconic(*38, 74, 75*). All mice

were maintained in specific-pathogen free facilities and used according to protocols approved by the Institutional Animal Care and Use Committee of TSRI-FL.

Naïve T-cell culture and transduction:

$CD8^+$ T cells were isolated from naïve mice using negative selection magnetic beads (StemCell). For primary TCR-mediated activation, purified $CD8^+$ T cells were plated at a density of $4x10^5$ cells/cm^2 at a concentration of $1x10^6$/mL and on plates pre-coated with goat anti-hamster capture antibody and media supplemented with hamster anti-CD3 (2C11) and anti-CD28 (37.51) (1ug/mL each). For retroviral transductions, 16 hours after initial plating, the T cell conditioned media was taken off, saved, and replaced with retroviral supernatants containing 10ug/mL polybrene, and the cultures were immediately centrifuged at ~ 500xg for 60 min at ~ 37 degrees C, followed by incubation for an additional 3 hours at 37 degrees C at 10% CO_2 incubator. Media containing retrovirus was aspirated and replaced with the saved conditions media. Cells were either transferred into mice (see infections) or continued to be cultured. For *in vitro* culturing, after 48 hours of total TCR stimulation, the activated cells were directly resuspended, counted, and re-cultured by diluting the cells into fresh media containing 10 or 100 U/mL rhIL-2 (NCI). Cells were re-cultured as $5x10^5$ cells/mL, every 24 hours following removal from the TCR stimulus(*38, 69*).

For experiments where cells were CTV labeled, after isolation, cells were pulsed with CTV for 10 minutes prior to activation.

Screening Analysis:

The geometric means from the live singlets transduced with shRNAmirs were measured via FACs. Control RNAis were used as the population reference to calculate individual Z scores at day 6 while the full population was used at day 3. From these Z scores a per shRNAmir percentile shift was calculated and averaged across all shRNAmirs targeting the same gene. These average shifts were used to calculated Z-scores, pvalues, and RNAi effects, which was calculated as $z * (1 - pvalue)$.

GSEA was computed on the RNAi effect values using cluster profiler(*76*) (Subramanian, 2005 #485}. Chromatin regulator family gene sets were custom built for this paper

Pathogens, infections, and colony forming assays:

LCMV-Armstrong and LCMV-Clone13 were produced as previously described (*77*). For experiments using in vitro transduced P14 cells, 50,000 activated cells were adoptively transferred into naïve C57/Bl6J mice r.o and an hour later infected with either 2×105 PFU of LCMV-Arm i.p. or 2x106 PFU r.o. For Listeria monocytogenes-GP33 (LM-GP33) was grown as previously described on brain heart infusion media(*78*). Mice were infected with 10,000 CFU for recall experiments.

Tumor transplant, ACT, and harvesting:

E0771 cells containing either a control MigR1-GFP or MigR1-GP33-GFP were cultured per providers instructions. For transplant, $1x10^6$ tumors cells per mouse were resuspended in 100µL of media and mixed 1:1 with 100uL of high concentration growth factor reduced (HC-GFR) matrigel (Corning) on ice and injected s.c. into mice mammary fat pads. 2 weeks later, $1x10^6$ P14 cells transduced with shRNAmirs were transferred into tumor bearing mice.

For harvesting, tumors were excised and dissociated into ~1cm pieces. Tumor were digested for 10 minutes in 10uL/mL DNAseI and 1uL/mL Collagenase and strained over a 70μM filter and spun for 10 minutes at 300g. Supernatant was then aspirated, and pellet was resuspended in 1mL of ACK lysis buffer for 5 minutes with occasional agitation. After 5 minutes, lysis buffer was diluted with 5 mL of cTCM and strained over a 45 μM filter and spun for 10 minutes at 300g. Pellets were then resuspended and spun in a 60/40 Percol gradient to specifically enrich lymphocytes.

B16 ACT experiments were performed as previously described(*79, 80*).

Ex-vivo isolation from tissues-spleen

For EdU experiments, mice were pulsed for either four hours (day 5) or overnight (day 8) with Edu before sacrifice.

T cells from mice infected with LCMV before day 6 were digested as previously reported(*81*). In brief, spleens were harvested into T-cell optimized media (cTCM)(*38*) and cut into ~1cm pieces. Spleens were digested for 10 minutes in 10uL/mL DNAseI and 1uL/mL Collagenase. Spleens were then treated as all other splenic experiments.

Spleens were strained over a 70μM filter and spun for 10 minutes at 300g. Supernatant was then aspirated, and pellet was resuspended in 1mL of ACK lysis buffer for 5 minutes with occasional agitation. After 5 minutes, lysis buffer was diluted with 5 mL of cTCM and strained over a 45 μM filter and spun for 10 minutes at 300g. For analytic flow cytometry, pellet was resuspended in 1mL of FACS buffer (1xPBS, 2% FBS, 10mM EDTA).

For sorting, cells were negatively isolated using a modified StemCell $CD8^+$ kit. In brief, biotinylated αCD19, αCD4,αB220,and αTER-20 antibodies were added to cell pellet in 1mL of cTCM and 50μL of rat serum. After 10 minutes, the manufactures instructions and reagents were followed and used. Cells were then transferred into FACS buffer for staining at ~30-40 million cells per mL (See staining protocol). After staining, cells were sorted via a BD Aria Fusion sorter.

Flow cytometry:

After tissue isolation, cell numbers were counted via an Acuri C6 or MACSQuant 10. Counts were normalized across individual mice to the highest number of P14 cells to reduce experimental variability. Samples were transferred into FACS buffer and stained for either 20 minutes at RT or 40 minutes at 4C. Samples were then washed and fixed for 10 minutes at 4 C in 4% PFA. Samples were washed again and placed into FACS buffer at 4 C until acquisition. Samples were acquired on a BD LSR2 or a Cytek Aurora

Generation of bulk RNA-seq libraries and sequencing

For bulk RNA-seq analysis of *in vivo* CTL, distinct phenotypic subsets were isolated by FACS and sorted into FBS coated DNA LoBind Eppendorf 1.5mL with 200uL of 1xPBS, 1mM DTT, and 5U of Recombinant RNAse inhibitors (Takara) , and then were washed in 1x PBS. Full-length CDNAs were generated directly from ~10,000 cells per sample using oligo(dT) priming and the SMART-Seq v4 Ultra Low Input RNA Kit (Clontech), and 150 pg of CDNA was used to prepare strand-specific paired-end sequencing libraries (Nextera XT, Illumina). Libraries were quantified using Qubit HS DNA assay (Invitrogen) and their quality was assessed on Agilent Technology 2100 Bioanalyzer using a High Sensitivity DNA chip (Agilent) and

dual-indexed pooled libraries were sequenced. Reads were aligned with salmon using validateMappings(*82*). Aligned reads were passed to DESEQ2 for differential gene analysis(*83*). All gene sets used were derived from previously published papers: EMP, naïve, and 48H(*1*); TE,MP,EE, and DP(*55*) ; T_{RM}, T_{CM}, and T_{EM} (*68*) Tcf7(*12*); and T_{prog}(*84*).

Nascent RNA-seq library preparation, sequencing, and data analysis were previously described(*1*)

Single cell clustering, cluster specific gene expression, and pseudotime analysis:

Single cell library preparation, sequencing, and alignment were previously described(*1*).

Single cell data was manipulated and analyzed first in the scanpy environment (*85*). Cells from D5 shCon, D5 shMll1, and D8 were down sampled to 800 cells and those matched to D3 to 400 cells. Mutual nearest neighbor batch correction was used to remove batch effect from the two separate sequencing experiments (mnn_correct) (*86*). Using the merged experiments, principal components (tl.pca) and nearest neighbors were calculated (pp.neighbors, neighbors=100, pcs=25) and then used to create Leiden clusters (tl.leiden, resolution =1). These clusters were then used to create a PAGA graph to estimate and simplify the connectivity of the clusters (tl.draw_graph) (*87*).

Data from these clusters was used for all single cell differential expression calculations using the Wilcoxon method (tl.rank_genes_groups). For GSEAs the score for each given analysis was used as the rank ordered input. To calculate pseudotime, an arbitrary D3 cell from Leiden cluster 7 (T1 in the text) was selected as the initial cell (tl.dpt).

RNA velocity, latent time, transitions, and dynamic genes:

To calculate RNA velocity, scvelo was used(*56*).First, using the pre-pseudotime PAGA analysis, neighbors, moments and initial velocity were calculated (pp.neighbors neighbors =100, pcs=50, pp.moments, and tl.velocity respectively). Next dynamic genes were recovered and used to compute the dynamical model (tl.recover_dynamics, tl.velocity). Using these dynamic genes both latent times (tl.latent_time) and ranked dynamic genes (tl.rank_dynamical_genes) were calculated. To calculate individual dynamic genes for either control or Mll1 deficent cells, cells originating from either Mll1 deficent or control samples were removed prior to scVelo analysis. These dynamic genes were then used to calculate transition probabilities.

Chromatin I.P: T cells were fixed in PBS containing a 1:10 ratio of fixation buffer (11.1% V/V MeOH free formaldehyde, 100mM NaCl, 1mM EDTA, and 50 mM Hepes pH7.5) for 15 minutes on ice. Fixation was quenched with a 1:20 addition of 2.5M glycine for an additional 15 minutes. Cells were then washed with PBS and nucli were extracted (10mM Tris pH7.5, 10mM EDTA, 150 mM NaCl, and 1% TritonX-100). Nucli were resuspended in lysis buffer (50mM Tris pH 8.0, 150mM NaCl, 1mM EDTA, 1% Nonidet P-40, 0.1% SDS, and 0.5% Deoxycholate, supplemented with protease and phosphate inhibitor tablets (Roche)). To make mono and di nucleosome size fragments for I.P, sonication was performed in covaris mini tubes for 30-45 minutes with following settings: peak power-160, duty factor -10, cycles/burst=200.

Before the addition of antibody, chromatin was brought up to 1mL total volume in lysis buffer and pre-cleared via the addition of 50uL of Protein G Dynabeads per 10^7 nucli equivalents at 4C for 2-3H. 5% of each reaction was then saved for making the input control. The equivalents of 10-20 million nucli were subdivided for each I.P per sample and brought up to 1mL total volume. Antibodies were then added to the chromatin and I.P'd for ~16-20H at 4C. Each sample was then conjugated to fresh Protein G Dynabeads

(5uL beads per 1ug of antibody) at RT for 15 minutes. After conjugation cells were washed twice with lysis buffer and once with TE. Decrosslinking than occurred via 30 minute treatment with RNAseA (100ug/mL) at 37C, followed by overnight digestion of protein via proteinase K (1mg/mL) at 65C(*88*).

For high resolution ChIP-Exo experiments, samples were washed as above and then ChIP-Exo 5.0 was followed as previously reported(*88*).

Library preparation and sequencing:

DNA from chromatin preps was extracted via phenol: chloroform extraction and then purified and concentrated via EtOH cleanup. Resulting DNA was quantified via Qubit. 1 to 5 ng of DNA were used to create sequencing libraries via NEB Ultra II DNA Kits. After amplification, resulting libraries were checked for size (~300bp) via either Bioanalyzer 2100 or TapeStation 4200. Samples were then pooled at equal molar amounts of library and concentrated/ size selected via AMPure beads. Library was then run on NEXT-Seq 500.

ChIP-Seq read processing and peak calling:

Reads from sequencing were trimmed using trim_galore (--paired --length 24 --stringency 3) and aligned to GRCm39 using bowtie2 (--no-mixed –no discordant)(*89*). Aligned reads were then trimmed for duplicates and quality using samtools (samtools view -f 2 -q 20 -h 473-1.sam | samtools sort -n -o $QualFilt -O bam; samtools fixmate -m $QualFilt $fixmate; samtools sort -O bam -o $fixsorted $fixmate; samtools markdup -r $fixsorted $dupremoved)(*90*). Peaks were then called both per replicate and for all replicates via macs 2(callpeak -t $duprembam -c $controlbam --broad -f BAMPE -g mm -q 0.05 -B)(*91*)

ChIP-Seq data processing:

To determine significant differences between given peaks, the r package DiffBind was used(*92*). In the context of replicate controlled samples (shCon/shMll1 H3K4me3 and RNApol2) an additional replicate factor was added as part of the design. Peaks with a pvalue <=0.05 were considered significant for this analysis.

To determine gene enrichment, peaks from the given sample were then annotated to the nearest gene using ChIPseeker (*93*). The number of these genes that overlapped with previously described gene sets were counted and the simple fraction of the whole of the gene set was visualized using ComplexHeatmap (*1, 2, 12, 45, 55, 80, 94-96*).

To compute per gene log2FCs of H3K4me3 binding, the reported peaks from Diffbind were collapsed to gene and log2fcs from multiple peaks per gene were averaged. (*92*). Using these and the Log2FCs computed via DESEQ2 for the previously published naRNA-seq, data values were plotted on a two way dot plot(*1, 83*). Genes were marked by their presence in previously described gene clusters that were differential across time(*45*).

To compute the enrichment of one set of peaks within another, bedtools was used to determine the number intersecting peaks. The fraction of intersecting peaks over total number was then computed.

To calculate the pausing rate we adapted a previously published strategy (*97*). Annotated genes were separated into their promoters (TSS +300,-50b.p) and proximal gene body (301-600 b.p) and the number of reads in either region were calculated. These were converted to transcripts per million and the sum of TPMs to promoter or gene body were calculated and averaged across replicates. The per gene promoter sum and the per gene body sum were then divided to form the pausing index. Differences between indices were calculated via KS test.

Supplementary Figures

Fig. S1. Chromatin regulators have both distinct and convergent effects on co-inhibitory gene expression

(**A**) Analytical method to compute and rank the average RNAi-induced effects (RNAi-effects) on marker protein expression in the screens that resulted from suppression of the same target gene with multiple distinct shRNAmirs. (**B**) Ranked RNAi-effects of each CRF in each screen are displayed as bar charts. Dashed lines indicate top and bottom 15th percentile of RNAi-effects. (**C**) GSEA shows the enrichment of genes encoding subunits that assemble in biochemically defined chromatin regulatory complexes CRFs (bottom) within RNAi-effects on marker proteins in each screen (left). RNAi-effect scores were used to calculate enrichment. (**D**) Correlogram shows relationship of CRF RNAi-effects on different protein markers in distinct culture conditions by computing the correlation between RNAi-effect scores for each marker protein in different culture conditions. Size and color of circles in each box denote correlation intensity and directionality.

Fig. S2. Mll1 deficiency coordinately decreases Tcf7 expression and increases co-inhibitory receptor expression

(**A**) Bar charts (*above*) indicate the mean expression of protein markers (gMFI) in cells transduced with all shRNAmirs specific for individual CRFs (or control genes) and for all shRNAmirs in the screen. Symbols indicate the individual raw gMFI values of cells transduced with unique shRNAmirs. P values were calculated using Welch's t-test. Histograms (*below*) show representative flow cytometry data for individual shRNAmirs specific for control genes or Mll1 in each screening condition. Numbers in plots indicate gMFI values. (**B**) Bar charts (*top*) and representative histograms (*bottom*) show marker protein expression in P14 Cas9-transgenic CD8 T cells transduced with sgRNAs targeting *Kmt2a* (symbols, n=3). Numbers in plots indicate gMFI.

Fig. S3. Mll1 deficient cells are not generally defective

(**A**) Mll1 expression was determined in whole cell lysates prepared from CD8 T cells transduced with either shRNAmirs (*left*) or sgRNAs (*right*). Transduced cells were purified by FACS three days after TCR activation and transduction. (**B**) Representative flow cytometry histograms from three biological replicates show *Tcf7*-GFP expression in $P14^{Tcf7\text{-GFP}}$ cells each day in culture after transduction with shCon or shMll1 shRNAmirs (*top*). The gMFI (*left*) and P values (*right*, paired t-test, comparisons from three biological replicates) are indicated in each plot and are summarized in the line graph (*bottom*, n=3). (**C**) Histograms show CTV labeling of naive P14 CD8 T cells (black) and its dilution after gating on cells transduced with shCon or shMll1 shRNAmirs each day after activation (*left*). Numbers on the plot show P values (paired t-test, from three biological replicates) after comparing the percent of shCon to shMll1 cells that fully diluted CTV, which is summarized in the line graph (*right*). (**D**) Histograms show cytokine expression detected by intracellular staining in cells transduced with control or Mll1 specific shRNAmirs after 6 days of culture in IL-2^{lo} or IL-2^{hi} conditions, followed by 4 hours of re-stimulation with phorbol 12-myristate 13-acetate

(PMA) and ionomycin. Numbers on the plot show the percent of cytokine positive cells (*top*) and the bar charts (*bottom*) summarize data as the means from four replicate experiments (P values, unpaired t-test).

Fig. S4. Mll1 restrains co-inhibitory protein expression and promotes formation of T_{prog} cells in the tumor microenvironment

(**A**) Schematics for the T cell adoptive transfer models using E0771 triple negative breast cancer (TNBC) (*top*) and B16 melanoma (*bottom*) tumors. (**B-C**) Representative flow cytometry plots from cells in mice transplanted with $E0771^{GP33}$ and $E0771^{GFP}$ in contralateral mammary fat pads after gating on CD8+ cells from different tissues (B, n=3), or $B16^{GP33}$ flank tumors (C, N=4), as well as their matched spleens (*top*). Numbers show percent of donor Thy1.1+ CD44+ (P14) cells (B) or percent of CD45.1 among gated CD8+ cells (C). Bar charts (*bottom*) summarize the mean percentage of total CD8+ cells and gMFI of PD-1 expression on P14 cells from mice (symbols) bearing E0771 (B) or B16 (C) tumors, and were compared using paired t-tests. (**D**) Representative flow cytometry plots after gating on P14 $CD8^+$ T cells transduced with shRNAmirs specific for negative control genes or Mll1 in $B16^{GP33}$ tumors, and comprise concatenated data from multiple mice (n=3). (**E**) Representative surface expression of PD-1 among $Tim3^{hi}$ P14 cells after gating on shCon or shMll1 transduced cells and is summarized by the bar charts as the means from individual mice (symbols) in multiple experiments. P values were calculated via paired t-test. (**F**) Bar charts show numbers of transduced P14 cells within $E0771^{GP33}$ (top) or $B16^{GP33}$ (bottom) tumors. The absolute numbers were normalized for $E0771^{GP33}$ at day 3 (left) or day 8 (right) pACT (Wilcoxon ranked-test). Accumulation in $B16^{GP33}$ bearing mice was calculated as the percent of CD8+ within $B16^{GP33}$ tumors at day 3 (*left*) or day 8 (*right*) pACT (paired t-test). (**G**) Line graph (top) shows control of $E0771^{GP33}$ tumors in recipients that received no adoptively transferred P14 cells (black), or P14 cells that were either shCon (grey) or shMll1 (blue) transduced. Each line shows the average growth of tumors smoothed over five days. Kaplan Myer curve (bottom) shows mice within this experiment reaching 1,500mm^3 tumor size. Significance was calculated using Mantel-Cox test. (**H**) Representative Tcf7-GFP expression in $P14^{Tcf7\text{-}GFP}$ $CD8^+$ T cells isolated from $E0771^{GP33}$ tumors after gating on cells transduced with shCon and shMll1 shRNAmirs (concatenated data from multiple mice, n=3). The gMFI values are indicated in each plot and their means for all mice (symbols) are summarized in the bar charts. P values calculated via paired t-test.

Fig. S5. Mll1 is necessary for persistence and formation of T_{prog} cells during chronic infections

(**A**) P14 cell accumulation in response to $LCMV_{Cl13}$. Symbols indicate normalized transduced P14 cell numbers in the spleen. Shaded portions of the plot indicate the normalized percent of transduced P14 cells of all $CD8^+$ cells. Both data present the mean of n≥3 individual mice. (**B**) Summary of T_{EX} development markers from Beltra, 2017, *Immunity(26)* (**C**) Flow cytometry plots show representative staining after gating on P14 $CD8^+$ T cells transduced with shCon and shMll shRNAmirs and comprise concatenated data from multiple mice (n=4). Bar charts summarize the mean frequencies of phenotypic T_{EX} cell populations from individual mice (symbols). P values calculated via Welch's t-test. (**D)** Representative expression of CX3CR1 within gated $Tim3^{hi}Tcf7^{lo}$ P14 cells comprises concatenated data from multiple mice (n=4). Bar charts summarize the means of individual mice (symbols). P values calculated via Welch's t-test.

Fig. S6. Mll1 promotes proliferation of responding T_{EFF} cells during primary infection

(A-D) Representative flow cytometry of transduced P14 $CD8^+$ T cells in the spleen after $LCMV_{Arm}$ infection are data concatenated from 2-5 mice. Values in the bar plots summarize the mean frequencies of the indicated phenotypic populations for all mice (symbols). P values were calculated with paired t-tests. (A) Representative KLRG1 staining on transduced P14 cells. (**B**) EdU incorporation is shown in the histogram after gating on P14 cells transduced with shCon or shMll1 shRNAmirs. (**C**) Representative

staining of KLRG1 and CD127 on P14-Cas9 CD8 T cells transduced with sgCon or sgKmt2a specific sgRNAs were analyzed on day 8 pi in the spleen. (**D**) EdU incorporation was measured as function of KLRG1 expression on day 8 pi, after gatining on P14 cells transduced with shCon or shMll1 shRNAmirs. (**E**) The absolute numbers of T_{CM}, T_{EM} and $T_{t\text{-}Tem}$ cells in the spleen after gating on shCon and shMll transduced P14 cells were quantified for multiple mice (symbols) 15 and 90 days after $LCMV_{Arm}$ infection. P values were calculated by Mann-Whitney test. (**F**) Experimental schema for analyzing the recall function and phenotype of primary memory cells that developed from shCon and shMll1 transduced P14 cells after initial $LCMV_{Arm}$ infection.

Fig. S7. Defective activation of MP and T_{SCM} gene expression by Mll1-deficient P14 cells early after $LCMV_{Arm}$ infection

(**A**) Experimental strategy for bulk RNA-seq of Mll1-deficient P14 cells. (**B**) Transcriptional differences on day 5 pi between wildtype (i.e., shCon-transduced) $KLRG1^{hi}$ and $KLRG1^{lo}$ P14 cells are depicted in the volcano plot. Genes whose expression was significantly different between the KLRG1 subsets that are more highly expressed in $Tcf7^{hi}$ (blue) or $Tcf7^{lo}$ (red) T_{EFF} cells from day 8 after $LCMV_{Arm}$ infection(*12*) were colored and specific signature genes were labeled. Bubble plots depict the relative enrichment of specific gene signatures in gene expression from $KLRG1^{hi}$ vs $KLRG1^{lo}$ cells (Wald statistic). (**C**) Volcano plots show the effect of Mll1 depletion in $KLRG1^{lo}$ (*top*) or $KLRG1^{hi}$ (*bottom*) P14 cells. Genes associated with $Tcf7^{hi}$ (blue) and $Tcf7^{lo}$ (red) cells were colored (*12*), and selected signature genes whose expression was significantly different were labelled.

Fig. S8. Mll1-deficient P14 cells inefficiently activate TCR-dependent genes whose transcriptional dynamics early during $LCMV_{Arm}$ infection establish development of T_{SCM} precursor cells.

(**A**) PAGA analysis of scRNA-seq data overlaid with pseudotime (left) and latent time (right). Pseudotime analysis was performed on all analyzed cells via SCANPY with a random cell in cluster T1 used as the starting node. Latent time was computed on all analyzed cells via scVelo. (**B**) Tables show cluster specific transition probabilities. Transition probabilities were calculated using data from cells isolated on days 3 and 8 pi, and separately for shCon (top) and shMll1 (bottom) cells that were isolated on day 5 pi with $LCMV_{Arm}$. (**C**) Bubble plots depict the enrichment of specific gene expression signatures (*left*) (*1, 2, 12, 45, 55, 68, 95*) in gene expression from shCon versus shMll1-transduced cells (Wilcoxon rank score) in each cluster. (**D**) Heatmap shows the $\log_2$ fold changes of a subset of T_{EFF} and T_{SCM} signature genes in each Lieden cluster versus all clusters (left), and whose expression differed significantly in shCon and shMll1-transduced cells in the trajectory (right) (Wilcoxon ranked p-value<=0.05). The genes were grouped thematically (labels) and clustered by Euclidean distance in the shMll1 vs. shCon comparison (right). (**E**) Barcode plot shows the GSEA of all shCon-transduced cell dynamic genes (10th percentile) in the comparison of all shMll1 vs shCon transduced cells. (**F**) Venn diagram shows overlap of the top dynamic genes (10th percentile) extracted from shCon or shMll1 cells in clusters T5 and T9 that explain their transition probabilities. (**G**) The presence of the top 10% of dynamic genes identified in either shCon and shMll1 transduced cells from clusters T5 and T9 among (top) all dynamic genes identified in shCon or shMll1 transduced cells from clusters T5 and T9 were determined, and those that were differentially expressed (p<=0.05), their differential expression shMll1 vs shCon transduced cells (bottom) from each cluster was plotted in the heatmap, which was ordered according to their expression between clusters T5 and T9 in shCon-transduced cells (middle).

Fig. S9. TCR stimulation and Mll1 coordinately establish transcriptional competence by inducing H3K4me3 at transcribed and poised of T_{MEM} cell genes

(A) The relative abundance of total and modified histones, Mll1-C and CTD modified RNA Pol II was examined by immunoblotting proteins from the insoluble portion of whole cell RIPA lysates from equivalent numbers of naive cells before and after TCR stimulation. (**B**) The overlaps between H3K4me3 ChIP-seq peaks in all examined CD8 T cell states (*left*), and specifically for those that exhibit increased H3K4me3 deposition in activated CD8 T cell states compared to naive cells (*right*) are shown in the Venn diagrams. Overlapping peaks had a minimum of one base pair overlap. (**C**) Bubble plot quantifies enrichment of differential gene expression (Wald statistic) from the indicated comparisons within genes harboring annotated H3K4me3 peaks that exhibited significantly increased or decreased H3K4me3 density in naive cells compared to TCR-activated or T_{MEM} (LM_{Ova} D60) cells (signatures).(**D**) Bubble plots show the enrichment of genes that exhibit differential H3K4me3 deposition after naive cell activation within specific gene expression signatures (labelled on left). Regions of differential H3K4me3 deposition in activated versus naive cells were annotated to the nearest gene and the average $\log_2$ fold change was calculated per gene and used for enrichment analysis. (**E**) The correlation between H3K4me3 deposition (y-axis) and chromatin-associated RNA expression (x-axis) in TCR stimulated versus naive P14 CD8 T cells is shown. Naive cells were stimulated for 24 (*left*) or 72 hours (*right*) before H3K4me3 ChIP-seq and for 24 (*left*) or 48 hours (*right*) before isolation of chromatin-associated RNA. The average $\log_2$ fold changes in H3K4me3 deposition and chromatin-associated RNA expression were calculated per gene and plotted. Signature genes previously identified as differentially expressed in $Tcf7^{hi}$ (red) or $Tcf7^{lo}$ (blue) T_{EFF} cells 8 days after $LCMV_{Arm}$ infection (*12*)(*top* plots) or involved in initial activation (red), naïve/memory cells (blue), or effector/memory cells (gold), were marked accordingly(*48, 98*) (*bottom* plots), and the number of genes from each category are indicated in each quadrant. R^2 values for each gene set and for all plotted genes (black) are indicated above each graph.

Fig. S10. Mll1 preferentially binds active TSSs and promotes transcription of genes *in vivo* that become transcriptionally paused upon TCR stimulation

(A) Violin plots show normalized counts of Pol II ChIP-seq reads from naïve (black) or activated (red) cells found in promoters or bodies of genes whose transcription is TCR dependent (*left*) or which have increased H3K4me3 in T_{MEM} relative to naïve cells. **(B)** The pausing indices of TCR dependent genes from naïve (black) and activated (red) cells are plotted as an eCDF. **(C)** Heatmaps show relative abundance ChIP-seq reads after mapping Mll1 (ChIP-exo5.0), H3K4me1 and H3K4me3 around accessible promoters and distal enhancers. Promoter regions are TSS's that are hyperaccessible (ATAC-seq) in activated $CD8^+$ T cells (*30*). Distal regions are those that are similarly open, but have a H3K4me1 mark deposited. **(D)** Violin plots show the number of molecules counted per encapsulated and sequenced cell during scRNA-seq. P value determined via Welch's unpaired t-test.

References:

1. H. Diao *et al.*, Single-cell lineage trajectories and chromatin regulators that initialize antiviral CD8 T cell ontogeny. *bioRxiv*, 2021.2008.2011.456014 (2021).
2. C. Yao *et al.*, Single-cell RNA-seq reveals TOX as a key regulator of CD8+ T cell persistence in chronic infection. *Nature Immunology* **20**, 890-901 (2019).
3. B. Kakaradov *et al.*, Early transcriptional and epigenetic regulation of CD8+ T cell differentiation revealed by single-cell RNA sequencing. *Nat Immunol* **18**, 422-432 (2017).
4. A. C. Richard *et al.*, T cell cytolytic capacity is independent of initial stimulation strength. *Nat Immunol* **19**, 849-858 (2018).
5. J. M. Marchingo *et al.*, T cell signaling. Antigen affinity, costimulation, and cytokine inputs sum linearly to amplify T cell expansion. *Science* **346**, 1123-1127 (2014).
6. D. Zehn, R. Thimme, E. Lugli, G. P. de Almeida, A. Oxenius, 'Stem-like' precursors are the fount to sustain persistent CD8(+) T cell responses. *Nat Immunol* **23**, 836-847 (2022).
7. S. C. Jameson, D. Masopust, Understanding Subset Diversity in T Cell Memory. *Immunity* **48**, 214-226 (2018).
8. S. M. Kaech, E. J. Wherry, Heterogeneity and cell-fate decisions in effector and memory CD8+ T cell differentiation during viral infection. *Immunity* **27**, 393-405 (2007).
9. L. M. McLane, M. S. Abdel-Hakeem, E. J. Wherry, CD8 T Cell Exhaustion During Chronic Viral Infection and Cancer. *Annu Rev Immunol* **37**, 457-495 (2019).

10. M. Philip, A. Schietinger, CD8(+) T cell differentiation and dysfunction in cancer. *Nat Rev Immunol* **22**, 209-223 (2022).
11. R. S. Akondy *et al.*, Origin and differentiation of human memory CD8 T cells after vaccination. *Nature* **552**, 362-367 (2017).
12. D. Pais Ferreira *et al.*, Central memory CD8(+) T cells derive from stem-like Tcf7(hi) effector cells in the absence of cytotoxic differentiation. *Immunity* **53**, 985-1000.e1011 (2020).
13. J. B. Johnnidis *et al.*, Inhibitory signaling sustains a distinct early memory CD8(+) T cell precursor that is resistant to DNA damage. *Sci Immunol* **6**, (2021).
14. P. Graef *et al.*, Serial transfer of single-cell-derived immunocompetence reveals stemness of CD8(+) central memory T cells. *Immunity* **41**, 116-126 (2014).
15. L. Gattinoni *et al.*, A human memory T cell subset with stem cell-like properties. *Nat Med* **17**, 1290-1297 (2011).
16. W. W. Lin *et al.*, CD8(+) T Lymphocyte Self-Renewal during Effector Cell Determination. *Cell Rep* **17**, 1773-1782 (2016).
17. X. Zhou *et al.*, Differentiation and persistence of memory CD8(+) T cells depend on T cell factor 1. *Immunity* **33**, 229-240 (2010).
18. A. G. Soerens *et al.*, Functional T cells are capable of supernumerary cell division and longevity. *Nature* **614**, 762-766 (2023).
19. W. H. Hudson *et al.*, Proliferating Transitory T Cells with an Effector-like Transcriptional Signature Emerge from PD-1(+) Stem-like CD8(+) T Cells during Chronic Infection. *Immunity* **51**, 1043-1058 e1044 (2019).
20. R. Zander *et al.*, CD4(+) T Cell Help Is Required for the Formation of a Cytolytic CD8(+) T Cell Subset that Protects against Chronic Infection and Cancer. *Immunity* **51**, 1028-1042 e1024 (2019).
21. D. T. Utzschneider *et al.*, T Cell Factor 1-Expressing Memory-like CD8+ T Cells Sustain the Immune Response to Chronic Viral Infections. *Immunity* **45**, 415-427 (2016).
22. S. J. Im *et al.*, Defining CD8+ T cells that provide the proliferative burst after PD-1 therapy. *Nature* **537**, 417-421 (2016).
23. R. He *et al.*, Follicular CXCR5-expressing CD8+ T cells curtail chronic viral infection. *Nature* **537**, 412-416 (2016).
24. R. Zander *et al.*, CD4(+) T Cell Help Is Required for the Formation of a Cytolytic CD8(+) T Cell Subset that Protects against Chronic Infection and Cancer. *Immunity* **51**, 1028-1042.e1024 (2019).
25. W. H. Hudson *et al.*, Proliferating Transitory T Cells with an Effector-like Transcriptional Signature Emerge from PD-1+ Stem-like CD8+ T Cells during Chronic Infection. *Immunity* **51**, 1043-1058.e1044 (2019).
26. J.-C. Beltra *et al.*, Developmental Relationships of Four Exhausted CD8+ T Cell Subsets Reveals Underlying Transcriptional and Epigenetic Landscape Control Mechanisms. *Immunity* **52**, 825-841.e828 (2020).
27. B. C. Miller *et al.*, Subsets of exhausted CD8(+) T cells differentially mediate tumor control and respond to checkpoint blockade. *Nat Immunol* **20**, 326-336 (2019).
28. K. E. Pauken *et al.*, Epigenetic stability of exhausted T cells limits durability of reinvigoration by PD-1 blockade. *Science* **354**, 1160-1165 (2016).
29. C. D. Scharer, A. P. Bally, B. Gandham, J. M. Boss, Cutting Edge: Chromatin Accessibility Programs CD8 T Cell Memory. *J Immunol* **198**, 2238-2243 (2017).
30. J. P. Scott-Browne *et al.*, Dynamic Changes in Chromatin Accessibility Occur in CD8(+) T Cells Responding to Viral Infection. *Immunity* **45**, 1327-1340 (2016).
31. B. Yu *et al.*, Epigenetic landscapes reveal transcription factors that regulate CD8(+) T cell differentiation. *Nature immunology* **18**, 573-582 (2017).
32. S. M. Gray, R. A. Amezquita, T. Guan, S. H. Kleinstein, S. M. Kaech, Polycomb Repressive Complex 2-Mediated Chromatin Repression Guides Effector CD8(+) T Cell Terminal Differentiation and Loss of Multipotency. *Immunity* **46**, 596-608 (2017).
33. B. Kakaradov *et al.*, Early transcriptional and epigenetic regulation of CD8(+) T cell differentiation revealed by single-cell RNA sequencing. *Nat Immunol* **18**, 422-432 (2017).
34. L. Pace *et al.*, The epigenetic control of stemness in CD8(+) T cell fate commitment. *Science* **359**, 177-186 (2018).
35. A. Guo *et al.*, cBAF complex components and MYC cooperate early in CD8(+) T cell fate. *Nature* **607**, 135-141 (2022).
36. D. T. Utzschneider *et al.*, Early precursor T cells establish and propagate T cell exhaustion in chronic infection. *Nat Immunol* **21**, 1256-1266 (2020).
37. E. Ahn *et al.*, Role of PD-1 during effector CD8 T cell differentiation. *Proc Natl Acad Sci U S A* **115**, 4749-4754 (2018).
38. M. E. Pipkin *et al.*, Interleukin-2 and inflammation induce distinct transcriptional programs that promote the differentiation of effector cytolytic T cells. *Immunity* **32**, 79-90 (2010).
39. B. K. Cenik, A. Shilatifard, COMPASS and SWI/SNF complexes in development and disease. *Nat Rev Genet* **22**, 38-58 (2021).
40. C. M. Hughes *et al.*, Menin associates with a trithorax family histone methyltransferase complex and with the hoxc8 locus. *Mol Cell* **13**, 587-597 (2004).
41. A. Yokoyama *et al.*, Leukemia proto-oncoprotein MLL forms a SET1-like histone methyltransferase complex with menin to regulate Hox gene expression. *Mol Cell Biol* **24**, 5639-5649 (2004).
42. J. Paggetti *et al.*, Crosstalk between leukemia-associated proteins MOZ and MLL regulates HOX gene expression in human cord blood CD34+ cells. *Oncogene* **29**, 5019-5031 (2010).

43. S. Denissov *et al.*, Mll2 is required for H3K4 trimethylation on bivalent promoters in embryonic stem cells, whereas Mll1 is redundant. *Development* **141**, 526-537 (2014).
44. Y. Ji *et al.*, Repression of the DNA-binding inhibitor Id3 by Blimp-1 limits the formation of memory CD8+ T cells. *Nature Immunology* **12**, 1230-1237 (2011).
45. J. A. Best *et al.*, Transcriptional insights into the CD8(+) T cell response to infection and memory T cell formation. *Nat Immunol* **14**, 404-412 (2013).
46. E. J. Wherry, J. N. Blattman, K. Murali-Krishna, R. van der Most, R. Ahmed, Viral persistence alters CD8 T-cell immunodominance and tissue distribution and results in distinct stages of functional impairment. *J Virol* **77**, 4911-4927 (2003).
47. S. M. Kaech, S. Hemby, E. Kersh, R. Ahmed, Molecular and functional profiling of memory CD8 T cell differentiation. *Cell* **111**, 837-851 (2002).
48. C. Y. Yang *et al.*, The transcriptional regulators Id2 and Id3 control the formation of distinct memory CD8+ T cell subsets. *Nat Immunol* **12**, 1221-1229 (2011).
49. W.-Hsuan W. Lin *et al.*, CD8+ T Lymphocyte Self-Renewal during Effector Cell Determination. *Cell Reports* **17**, 1773-1782 (2016).
50. V. Kalia *et al.*, Prolonged interleukin-2Ralpha expression on virus-specific CD8+ T cells favors terminal-effector differentiation in vivo. *Immunity* **32**, 91-103 (2010).
51. N. S. Joshi *et al.*, Inflammation directs memory precursor and short-lived effector CD8(+) T cell fates via the graded expression of T-bet transcription factor. *Immunity* **27**, 281-295 (2007).
52. C. Gerlach *et al.*, The chemokine receptor CX3CR1 defines three antigen-experienced CD8 T cell subsets with distinct roles in immune surveillance and homeostasis. *Immunity* **45**, 1270-1284 (2016).
53. J. J. Obar, K. M. Khanna, L. Lefrançois, Endogenous naive CD8+ T cell precursor frequency regulates primary and memory responses to infection. *Immunity* **28**, 859-869 (2008).
54. E. J. Wherry *et al.*, Lineage relationship and protective immunity of memory CD8 T cell subsets. *Nature immunology* **4**, 225-234 (2003).
55. D. Wang *et al.*, The Transcription Factor Runx3 Establishes Chromatin Accessibility of cis-Regulatory Landscapes that Drive Memory Cytotoxic T Lymphocyte Formation. *Immunity* **48**, 659-674.e656 (2018).
56. V. Bergen, M. Lange, S. Peidli, F. A. Wolf, F. J. Theis, Generalizing RNA velocity to transient cell states through dynamical modeling. *Nature Biotechnology* **38**, 1408-1414 (2020).
57. M. G. Guenther, S. S. Levine, L. A. Boyer, R. Jaenisch, R. A. Young, A Chromatin Landmark and Transcription Initiation at Most Promoters in Human Cells. *Cell* **130**, 77-88 (2007).
58. H. Wang *et al.*, H3K4me3 regulates RNA polymerase II promoter-proximal pause-release. *Nature* **615**, 339-348 (2023).
59. B. E. Russ *et al.*, Distinct epigenetic signatures delineate transcriptional programs during virus-specific CD8(+) T cell differentiation. *Immunity* **41**, 853-865 (2014).
60. T. A. Milne *et al.*, MLL Targets SET Domain Methyltransferase Activity to Hox Gene Promoters. *Molecular Cell* **10**, 1107-1117 (2002).
61. T. Nakamura *et al.*, ALL-1 Is a Histone Methyltransferase that Assembles a Supercomplex of Proteins Involved in Transcriptional Regulation. *Molecular Cell* **10**, 1119-1128 (2002).
62. P. Wang *et al.*, Global analysis of H3K4 methylation defines MLL family member targets and points to a role for MLL1-mediated H3K4 methylation in the regulation of transcriptional initiation by RNA polymerase II. *Mol Cell Biol* **29**, 6074-6085 (2009).
63. M. Wu *et al.*, Molecular regulation of H3K4 trimethylation by Wdr82, a component of human Set1/COMPASS. *Mol Cell Biol* **28**, 7337-7344 (2008).
64. J. J. Milner *et al.*, Delineation of a molecularly distinct terminally differentiated memory CD8 T cell population. *Proc Natl Acad Sci U S A* **117**, 25667-25678 (2020).
65. M. J. Rossi, W. K. M. Lai, B. F. Pugh, Simplified ChIP-exo assays. *Nat Commun* **9**, 2842 (2018).
66. E.-J. Cho, T. Takagi, C. R. Moore, S. Buratowski, mRNA capping enzyme is recruited to the transcription complex by phosphorylation of the RNA polymerase II carboxy-terminal domain. *Genes & development* **11**, 3319-3326 (1997).
67. H. H. Ng, F. Robert, R. A. Young, K. Struhl, Targeted recruitment of Set1 histone methylase by elongating Pol II provides a localized mark and memory of recent transcriptional activity. *Mol Cell* **11**, 709-719 (2003).
68. L. K. Mackay *et al.*, Hobit and Blimp1 instruct a universal transcriptional program of tissue residency in lymphocytes. *Science* **352**, 459-463 (2016).
69. R. Chen *et al.*, In vivo RNA interference screens identify regulators of antiviral CD4(+) and CD8(+) T cell differentiation. *Immunity* **41**, 325-338 (2014).
70. C. Fellmann *et al.*, An Optimized microRNA Backbone for Effective Single-Copy RNAi. *Cell Reports* **5**, 1704-1713 (2013).
71. Simon R. V. Knott *et al.*, A Computational Algorithm to Predict shRNA Potency. *Molecular Cell* **56**, 796-807.
72. K. Labun *et al.*, CHOPCHOP v3: expanding the CRISPR web toolbox beyond genome editing. *Nucleic Acids Research* **47**, W171-W174 (2019).
73. Q. Yang *et al.*, TCF-1 upregulation identifies early innate lymphoid progenitors in the bone marrow. *Nature Immunology* **16**, 1044-1050 (2015).

74. H. Pircher, K. Burki, R. Lang, H. Hengartner, R. M. Zinkernagel, Tolerance induction in double specific T-cell receptor transgenic mice varies with antigen. *Nature* **342**, 559-561 (1989).
75. P. Mombaerts *et al.*, Mutations in T-cell antigen receptor genes α and β block thymocyte development at different stages. *Nature* **360**, 225-231 (1992).
76. clusterProfiler: an R Package for Comparing Biological Themes Among Gene Clusters. *OMICS: A Journal of Integrative Biology* **16**, 284-287 (2012).
77. R. Ahmed, A. Salmi, L. D. Butler, J. M. Chiller, M. B. Oldstone, Selection of genetic variants of lymphocytic choriomeningitis virus in spleens of persistently infected mice. Role in suppression of cytotoxic T lymphocyte response and viral persistence. *J Exp Med* **160**, 521-540 (1984).
78. J. A. Olson, C. McDonald-Hyman, S. C. Jameson, S. E. Hamilton, Effector-like CD8(+) T cells in the memory population mediate potent protective immunity. *Immunity* **38**, 1250-1260 (2013).
79. J. J. Milner *et al.*, Bromodomain protein BRD4 directs and sustains CD8 T cell differentiation during infection. *J Exp Med* **218**, (2021).
80. J. J. Milner *et al.*, Runx3 programs CD8+ T cell residency in non-lymphoid tissues and tumours. *Nature* **552**, 253 (2017).
81. L. B. Rodda *et al.*, Single-Cell RNA Sequencing of Lymph Node Stromal Cells Reveals Niche-Associated Heterogeneity. *Immunity* **48**, 1014-1028.e1016 (2018).
82. R. Patro, G. Duggal, M. I. Love, R. A. Irizarry, C. Kingsford, Salmon: fast and bias-aware quantification of transcript expression using dual-phase inference. *Nature methods* **14**, 417-419 (2017).
83. M. I. Love, W. Huber, S. Anders, Moderated estimation of fold change and dispersion for RNA-seq data with DESeq2. *Genome Biol* **15**, 550 (2014).
84. C. Yao *et al.*, Single-cell RNA-seq reveals TOX as a key regulator of CD8(+) T cell persistence in chronic infection. *Nat Immunol* **20**, 890-901 (2019).
85. F. A. Wolf, P. Angerer, F. J. Theis, SCANPY: large-scale single-cell gene expression data analysis. *Genome Biology* **19**, 15 (2018).
86. L. Haghverdi, A. T. L. Lun, M. D. Morgan, J. C. Marioni, Batch effects in single-cell RNA-sequencing data are corrected by matching mutual nearest neighbors. *Nature Biotechnology* **36**, 421-427 (2018).
87. F. A. Wolf *et al.*, PAGA: graph abstraction reconciles clustering with trajectory inference through a topology preserving map of single cells. *Genome Biology* **20**, 59 (2019).
88. M. J. Rossi, W. K. M. Lai, B. F. Pugh, Simplified ChIP-exo assays. *Nature Communications* **9**, 2842 (2018).
89. B. Langmead, S. L. Salzberg, Fast gapped-read alignment with Bowtie 2. *Nat Methods* **9**, 357-359 (2012).
90. P. Danecek *et al.*, Twelve years of SAMtools and BCFtools. *Gigascience* **10**, (2021).
91. Y. Zhang *et al.*, Model-based Analysis of ChIP-Seq (MACS). *Genome Biology* **9**, R137 (2008).
92. C. S. Ross-Innes *et al.*, Differential oestrogen receptor binding is associated with clinical outcome in breast cancer. *Nature* **481**, 389-393 (2012).
93. G. Yu, L.-G. Wang, Q.-Y. He, ChIPseeker: an R/Bioconductor package for ChIP peak annotation, comparison and visualization. *Bioinformatics* **31**, 2382-2383 (2015).
94. C. X. Dominguez *et al.*, The transcription factors ZEB2 and T-bet cooperate to program cytotoxic T cell terminal differentiation in response to LCMV viral infection. *J Exp Med* **212**, 2041-2056 (2015).
95. A. Xin *et al.*, A molecular threshold for effector CD8(+) T cell differentiation controlled by transcription factors Blimp-1 and T-bet. *Nat Immunol* **17**, 422-432 (2016).
96. Z. Gu, R. Eils, M. Schlesner, Complex heatmaps reveal patterns and correlations in multidimensional genomic data. *Bioinformatics* **32**, 2847-2849 (2016).
97. P. B. Rahl *et al.*, c-Myc regulates transcriptional pause release. *Cell* **141**, 432-445 (2010).
98. H. Diao, M. Pipkin, Stability and flexibility in chromatin structure and transcription underlies memory CD8 T-cell differentiation [version 1; peer review: 2 approved]. *F1000Research* **8**, (2019).

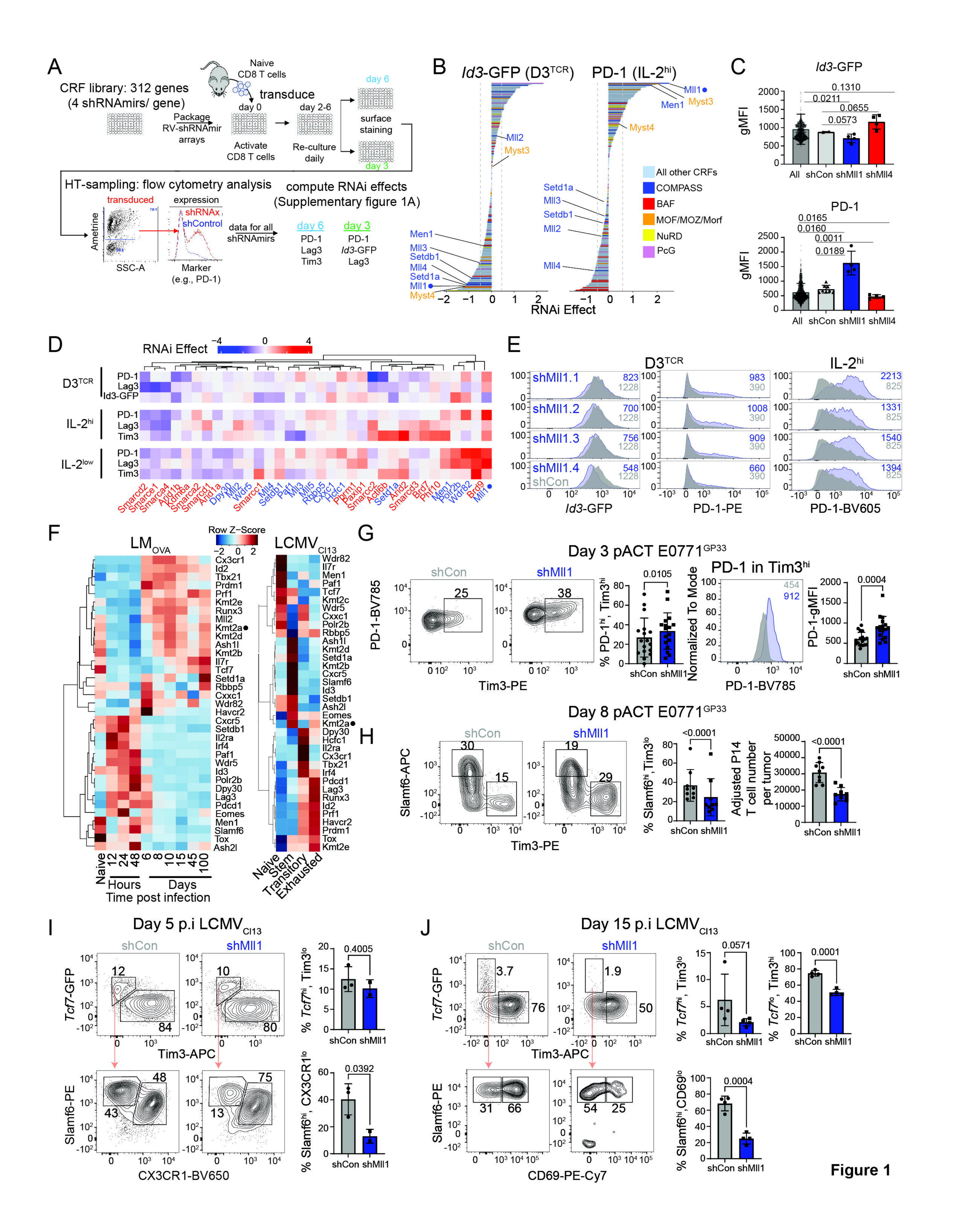
A
CRF library: 312 genes
(4 shRNAmirs/ gene)
Naive
CD8 T cells
transduce
Package
RV-shRNAmir
arrays
day 0
Activate
CD8 T cells
day 2-6
Re-culture
daily
day 6
surface
staining
day 3
HT-sampling: flow cytometry analysis
transduced
expression
shRNAx
shControl
Ametrine
SSC-A
Marker
(e.g., PD-1)
data for all
shRNAmirs
compute RNAi effects
(Supplementary figure 1A)
day 6
PD-1
Lag3
Tim3
day 3
PD-1
Id3-GFP
Lag3
B
Id3-GFP (D3TCR)
PD-1 (IL-2hi)
RNAi Effect
All other CRFs
COMPASS
BAF
MOF/MOZ/Morf
NuRD
PcG
C
Id3-GFP
gMFI
All
shCon
shMll1
shMll4
PD-1
D
RNAi Effect
D3TCR
IL-2hi
IL-2low
PD-1
Lag3
Id3-GFP
Tim3
E
D3TCR
IL-2hi
shMll1.1
shMll1.2
shMll1.3
shMll1.4
shCon
Id3-GFP
PD-1-PE
PD-1-BV605
F
LMOVA
LCMVCl13
Row Z-Score
Naive
Stem
Transitory
Exhausted
Hours
Days
Time post infection
G
Day 3 pACT E0771GP33
shCon
shMll1
PD-1-BV785
Tim3-PE
% PD-1hi, Tim3hi
PD-1 in Tim3hi
Normalized To Mode
PD-1-gMFI
H
Day 8 pACT E0771GP33
Slamf6-APC
% Slamf6hi, Tim3lo
Adjusted P14
T cell number
per tumor
I
Day 5 p.i LCMVCl13
Tcf7-GFP
Tim3-APC
Slamf6-PE
CX3CR1-BV650
% Tcf7hi, Tim3lo
% Slamf6hi, CX3CR1lo
J
Day 15 p.i LCMVCl13
% Tcf7hi, Tim3lo
% Tcf7lo, Tim3hi
% Slamf6hi, CD69lo
CD69-PE-Cy7

Figure 1

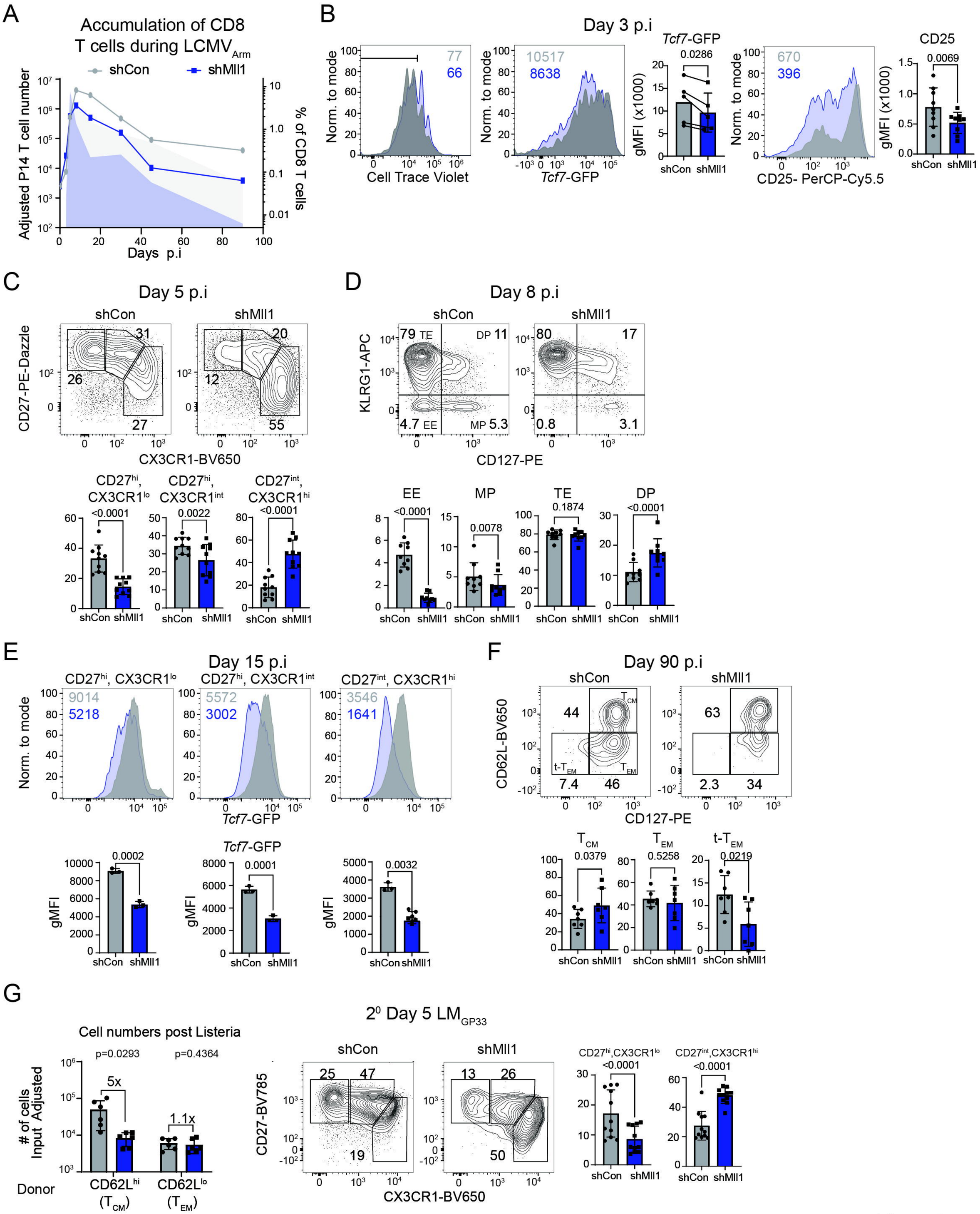
A
Accumulation of CD8 T cells during LCMV$_{Arm}$
shCon
shMll1
Adjusted P14 T cell number
% of CD8 T cells
Days p.i
B
Day 3 p.i
Norm. to mode
Cell Trace Violet
77
66
10517
8638
Tcf7-GFP
gMFI (x1000)
0.0286
670
396
CD25- PerCP-Cy5.5
CD25
0.0069
C
Day 5 p.i
CD27-PE-Dazzle
CX3CR1-BV650
31
26
27
20
12
55
CD27hi, CX3CR1lo
CD27hi, CX3CR1int
CD27int, CX3CR1hi
<0.0001
0.0022
D
Day 8 p.i
KLRG1-APC
CD127-PE
79 TE
DP 11
4.7 EE
MP 5.3
80
17
0.8
3.1
EE
MP
TE
DP
0.1874
0.0078
E
Day 15 p.i
9014
5218
5572
3002
3546
1641
0.0002
0.0001
0.0032
F
Day 90 p.i
CD62L-BV650
44
46
7.4
63
34
2.3
TCM
TEM
t-TEM
0.0379
0.5258
0.0219
G
Cell numbers post Listeria
p=0.0293
p=0.4364
5x
1.1x
# of cells Input Adjusted
Donor
CD62Lhi (TCM)
CD62Llo (TEM)
2⁰ Day 5 LMGP33
CD27-BV785
25
47
19
13
26
50
CD27hi,CX3CR1lo
CD27int,CX3CR1hi

Figure 2

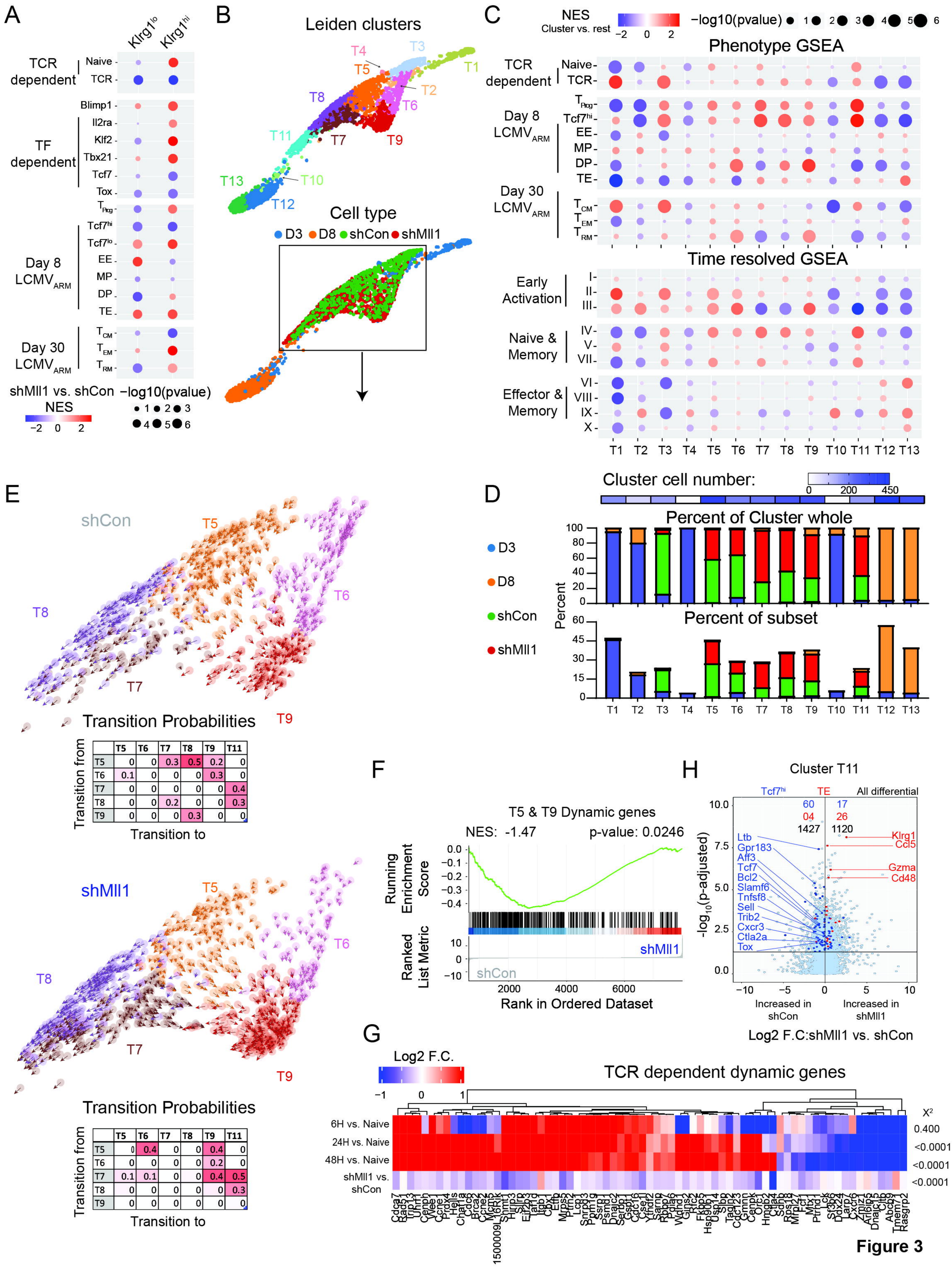
A
Klrg1lo
Klrg1hi
TCR dependent
Naive
TCR
TF dependent
Blimp1
Il2ra
Klf2
Tbx21
Tcf7
Tox
Day 8 LCMVARM
TProg
Tcf7hi
Tcf7lo
EE
MP
DP
TE
Day 30 LCMVARM
TCM
TEM
TRM
shMll1 vs. shCon
NES
−log10(pvalue)
B
Leiden clusters
Cell type
D3
D8
shCon
shMll1
C
NES
Cluster vs. rest
−log10(pvalue)
Phenotype GSEA
Time resolved GSEA
Early Activation
Naive & Memory
Effector & Memory
D
Cluster cell number:
Percent of Cluster whole
Percent of subset
Percent
E
shCon
shMll1
Transition Probabilities
Transition from
Transition to
F
T5 & T9 Dynamic genes
NES: -1.47
p-value: 0.0246
Running Enrichment Score
Ranked List Metric
Rank in Ordered Dataset
H
Cluster T11
All differential
Increased in shCon
Increased in shMll1
Log2 F.C:shMll1 vs. shCon
G
Log2 F.C.
TCR dependent dynamic genes
6H vs. Naive
24H vs. Naive
48H vs. Naive
shMll1 vs. shCon
X2

Figure 3

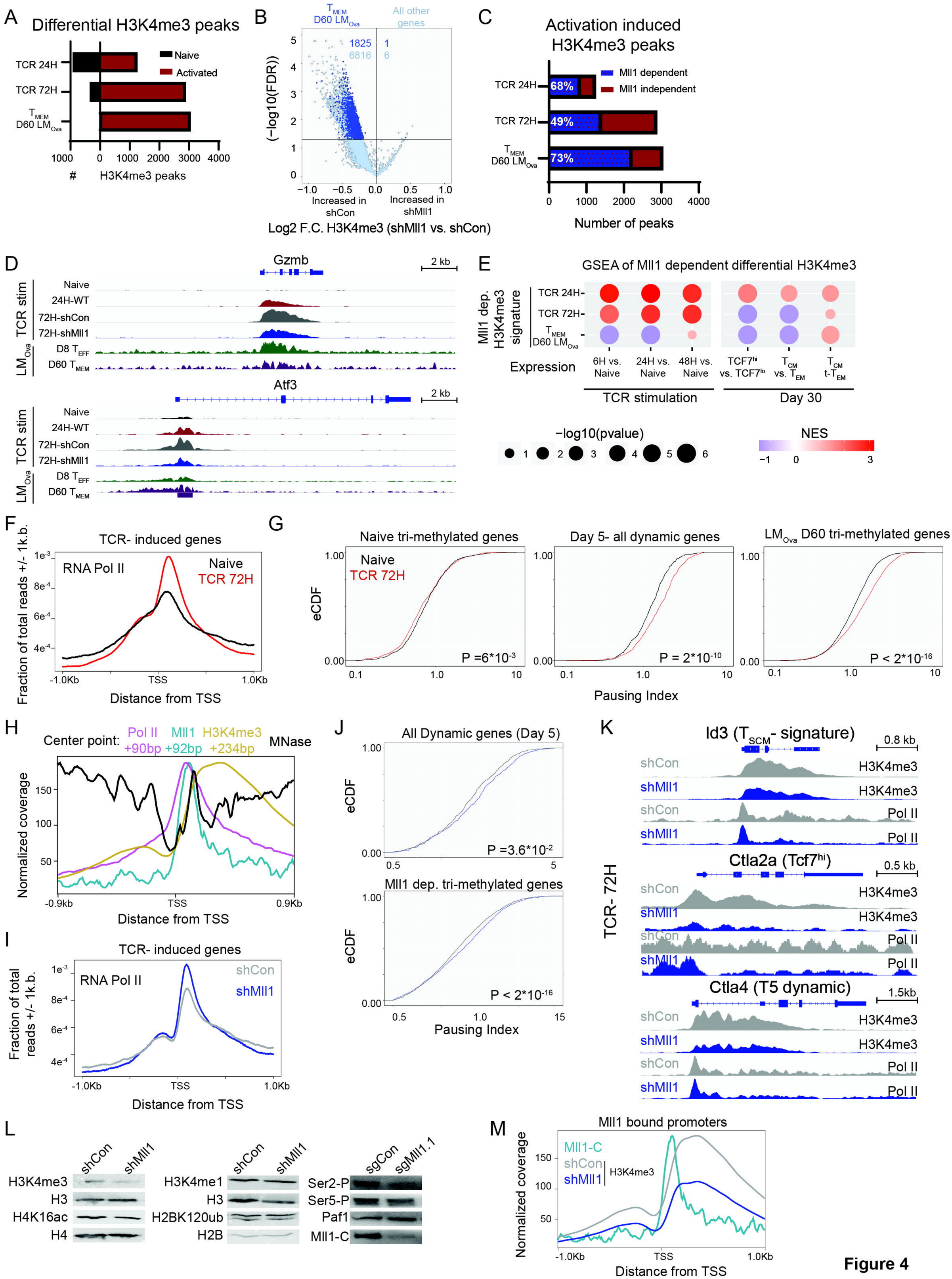
A
Differential H3K4me3 peaks
Naive
Activated
TCR 24H
TCR 72H
T MEM D60 LM Ova
1000 0 1000 2000 3000 4000
H3K4me3 peaks
B
T MEM D60 LM Ova
All other genes
1825
6816
1
6
(−log10(FDR))
Increased in shCon
Increased in shMll1
Log2 F.C. H3K4me3 (shMll1 vs. shCon)
C
Activation induced H3K4me3 peaks
Mll1 dependent
Mll1 independent
68%
49%
73%
Number of peaks
D
Gzmb
2 kb
Naive
24H-WT
72H-shCon
72H-shMll1
D8 T EFF
D60 T MEM
TCR stim
LM Ova
Atf3
E
GSEA of Mll1 dependent differential H3K4me3
Mll1 dep. H3K4me3 signature
Expression
6H vs. Naive
24H vs. Naive
48H vs. Naive
TCF7hi vs. TCF7lo
T CM vs. T EM
T CM t-T EM
TCR stimulation
Day 30
−log10(pvalue)
NES
F
TCR- induced genes
RNA Pol II
Naive
TCR 72H
Fraction of total reads +/- 1k.b.
Distance from TSS
G
Naive tri-methylated genes
Day 5- all dynamic genes
LM Ova D60 tri-methylated genes
eCDF
P =6*10-3
P = 2*10-10
P < 2*10-16
Pausing Index
H
Center point:
Pol II +90bp
Mll1 +92bp
H3K4me3 +234bp
MNase
Normalized coverage
Distance from TSS
I
TCR- induced genes
RNA Pol II
shCon
shMll1
Fraction of total reads +/- 1k.b.
Distance from TSS
J
All Dynamic genes (Day 5)
P =3.6*10-2
Mll1 dep. tri-methylated genes
P < 2*10-16
Pausing Index
K
Id3 (T SCM- signature)
0.8 kb
Ctla2a (Tcf7hi)
0.5 kb
Ctla4 (T5 dynamic)
1.5kb
TCR- 72H
H3K4me3
Pol II
L
shCon
shMll1
sgCon
sgMll1.1
H3K4me3
H3
H4K16ac
H4
H3K4me1
H2BK120ub
H2B
Ser2-P
Ser5-P
Paf1
Mll1-C
M
Mll1 bound promoters
Mll1-C
shCon
shMll1
H3K4me3
Normalized coverage
Distance from TSS

Figure 4

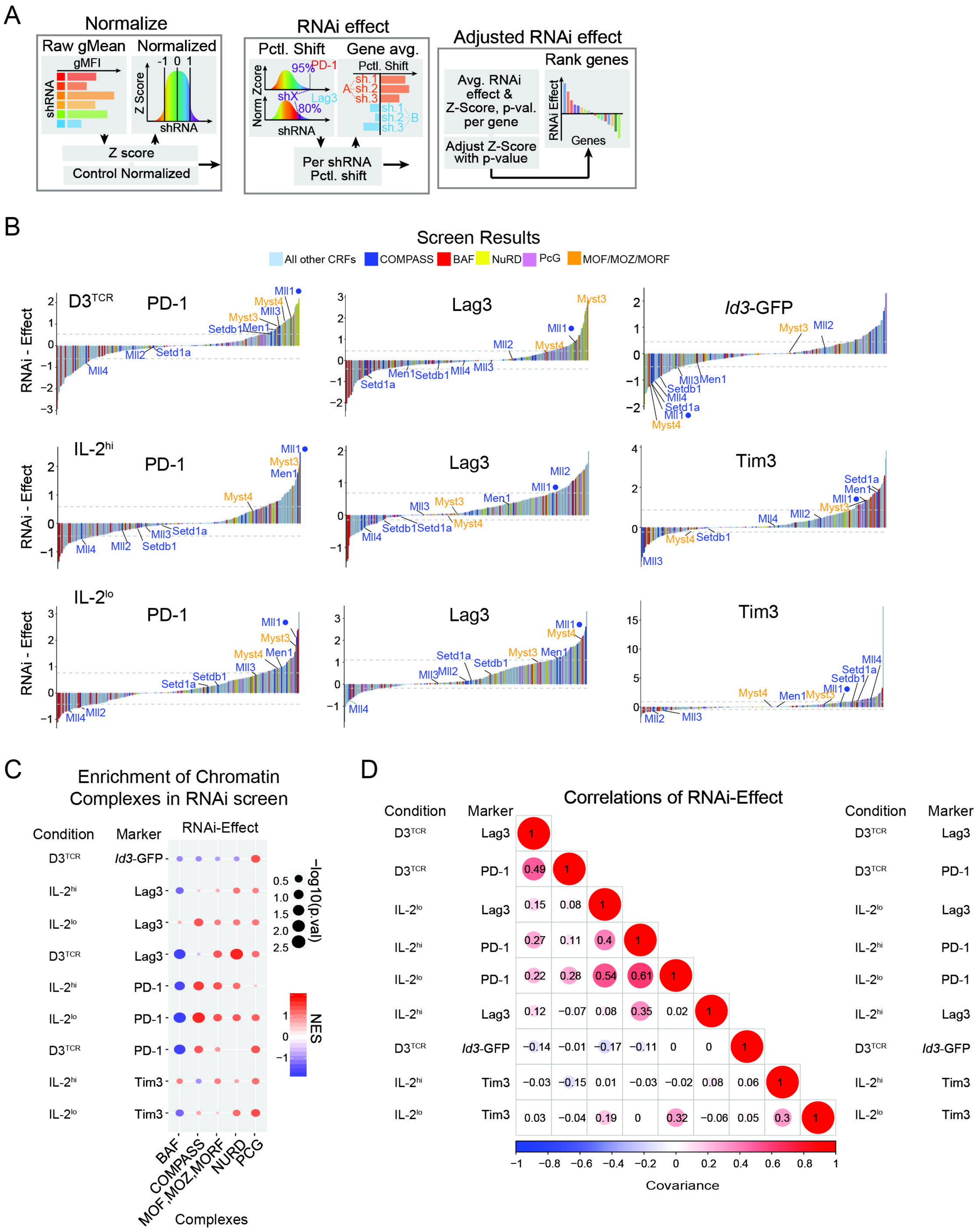
A
Normalize
Raw gMean
Normalized
gMFI
shRNA
Z Score
Z score
Control Normalized
RNAi effect
Pctl. Shift
Gene avg.
95%
PD-1
shX
Lag3
80%
Norm Zcore
Per shRNA Pctl. shift
Adjusted RNAi effect
Rank genes
Avg. RNAi effect & Z-Score, p-val. per gene
Adjust Z-Score with p-value
RNAi Effect
Genes
B
Screen Results
All other CRFs
COMPASS
BAF
NuRD
PcG
MOF/MOZ/MORF
D3TCR
PD-1
Lag3
Id3-GFP
IL-2hi
Tim3
IL-2lo
RNAi - Effect
C
Enrichment of Chromatin Complexes in RNAi screen
Condition
Marker
RNAi-Effect
−log10(p.val)
NES
BAF
COMPASS
MOF,MOZ,MORF
NURD
PCG
Complexes
D
Correlations of RNAi-Effect
Covariance

Sup. Figure 1

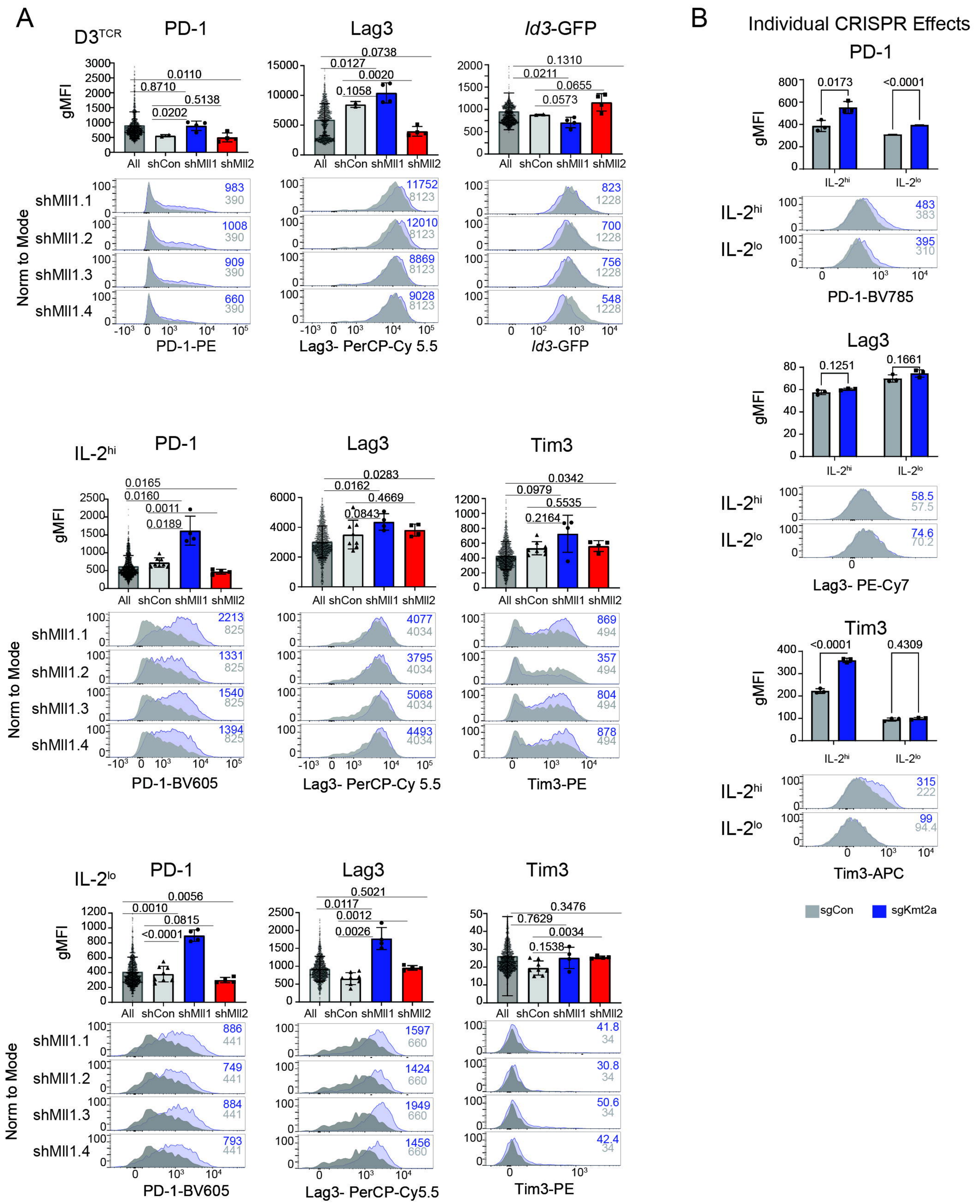
A
D3TCR
PD-1
Lag3
Id3-GFP
gMFI
All shCon shMll1 shMll2
Norm to Mode
shMll1.1
shMll1.2
shMll1.3
shMll1.4
PD-1-PE
Lag3- PerCP-Cy 5.5
Id3-GFP
IL-2hi
PD-1
Lag3
Tim3
PD-1-BV605
Lag3- PerCP-Cy 5.5
Tim3-PE
IL-2lo
PD-1
Lag3
Tim3
PD-1-BV605
Lag3- PerCP-Cy5.5
Tim3-PE
B
Individual CRISPR Effects
PD-1
IL-2hi
IL-2lo
PD-1-BV785
Lag3
Lag3- PE-Cy7
Tim3
Tim3-APC
sgCon
sgKmt2a

Sup. Figure 2

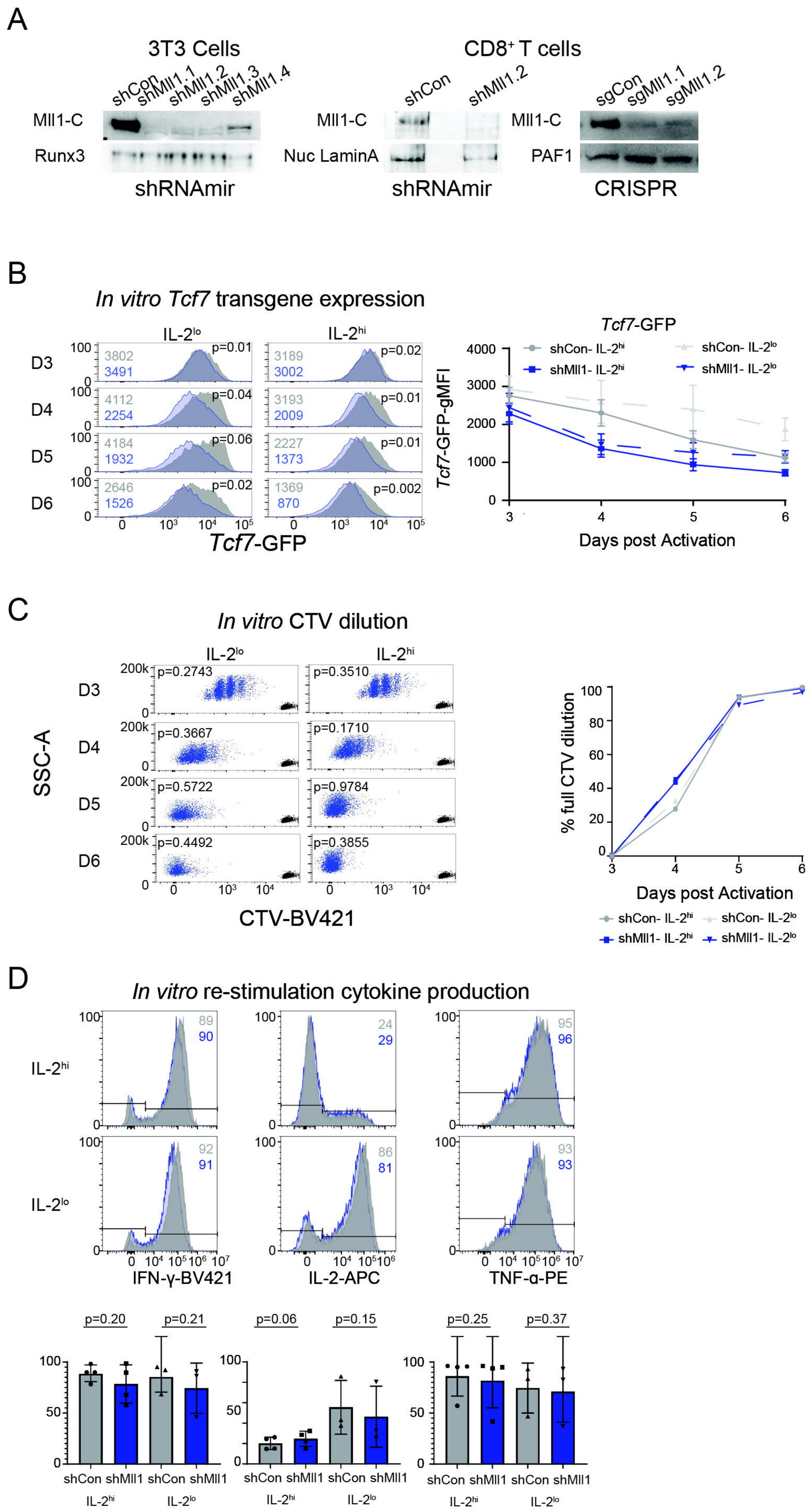
A
3T3 Cells
shCon
shMll1.1
shMll1.2
shMll1.3
shMll1.4
Mll1-C
Runx3
shRNAmir
CD8+ T cells
shCon
shMll1.2
Mll1-C
Nuc LaminA
shRNAmir
sgCon
sgMll1.1
sgMll1.2
Mll1-C
PAF1
CRISPR
B
In vitro Tcf7 transgene expression
IL-2lo
IL-2hi
D3
D4
D5
D6
3802
3491
p=0.01
3189
3002
p=0.02
4112
2254
p=0.04
3193
2009
p=0.01
4184
1932
p=0.06
2227
1373
p=0.01
2646
1526
p=0.02
1369
870
p=0.002
Tcf7-GFP
Tcf7-GFP
Tcf7-GFP-gMFI
shCon- IL-2hi
shMll1- IL-2hi
shCon- IL-2lo
shMll1- IL-2lo
Days post Activation
C
In vitro CTV dilution
IL-2lo
IL-2hi
SSC-A
D3
D4
D5
D6
p=0.2743
p=0.3510
p=0.3667
p=0.1710
p=0.5722
p=0.9784
p=0.4492
p=0.3855
CTV-BV421
% full CTV dilution
Days post Activation
shCon- IL-2hi
shCon- IL-2lo
shMll1- IL-2hi
shMll1- IL-2lo
D
In vitro re-stimulation cytokine production
IL-2hi
IL-2lo
89
90
24
29
95
96
92
91
86
81
93
93
IFN-γ-BV421
IL-2-APC
TNF-α-PE
p=0.20
p=0.21
p=0.06
p=0.15
p=0.25
p=0.37
shCon shMll1 shCon shMll1
IL-2hi
IL-2lo

Sup. Figure 3

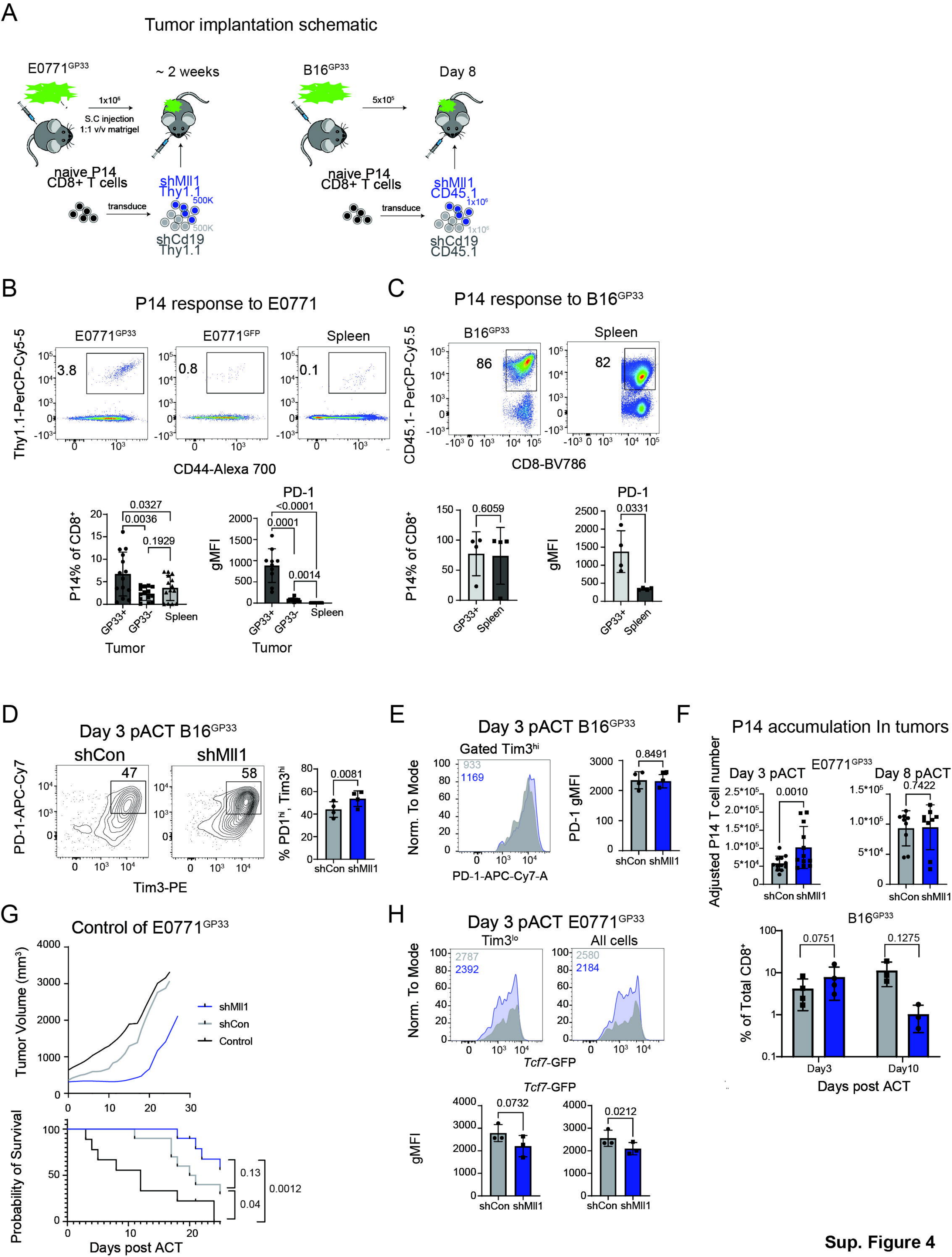
A
Tumor implantation schematic
E0771GP33
~ 2 weeks
1x10^6
S.C injection
1:1 v/v matrigel
naive P14
CD8+ T cells
shMll1
Thy1.1
500K
transduce
500K
shCd19
Thy1.1
B16GP33
Day 8
5x10^5
naive P14
CD8+ T cells
shMll1
CD45.1
1x10^6
transduce
1x10^6
shCd19
CD45.1
B
P14 response to E0771
E0771GP33
E0771GFP
Spleen
Thy1.1-PerCP-Cy5-5
CD44-Alexa 700
3.8
0.8
0.1
P14% of CD8+
0.0327
0.0036
0.1929
GP33+
GP33-
Spleen
Tumor
PD-1
gMFI
<0.0001
0.0001
0.0014
C
P14 response to B16GP33
B16GP33
Spleen
CD45.1- PerCP-Cy5.5
CD8-BV786
86
82
P14% of CD8+
0.6059
PD-1
gMFI
0.0331
GP33+
Spleen
D
Day 3 pACT B16GP33
shCon
shMll1
PD-1-APC-Cy7
Tim3-PE
47
58
% PD1hi, Tim3hi
0.0081
shCon shMll1
E
Day 3 pACT B16GP33
Gated Tim3hi
933
1169
Norm. To Mode
PD-1-APC-Cy7-A
PD-1 gMFI
0.8491
shCon shMll1
F
P14 accumulation In tumors
E0771GP33
Day 3 pACT
Day 8 pACT
Adjusted P14 T cell number
0.0010
0.7422
shCon shMll1
B16GP33
% of Total CD8+
0.0751
0.1275
Day3
Day10
Days post ACT
G
Control of E0771GP33
Tumor Volume (mm3)
shMll1
shCon
Control
Probability of Survival
0.13
0.04
0.0012
Days post ACT
H
Day 3 pACT E0771GP33
Tim3lo
All cells
2787
2392
2580
2184
Norm. To Mode
Tcf7-GFP
gMFI
0.0732
0.0212
shCon shMll1

Sup. Figure 4

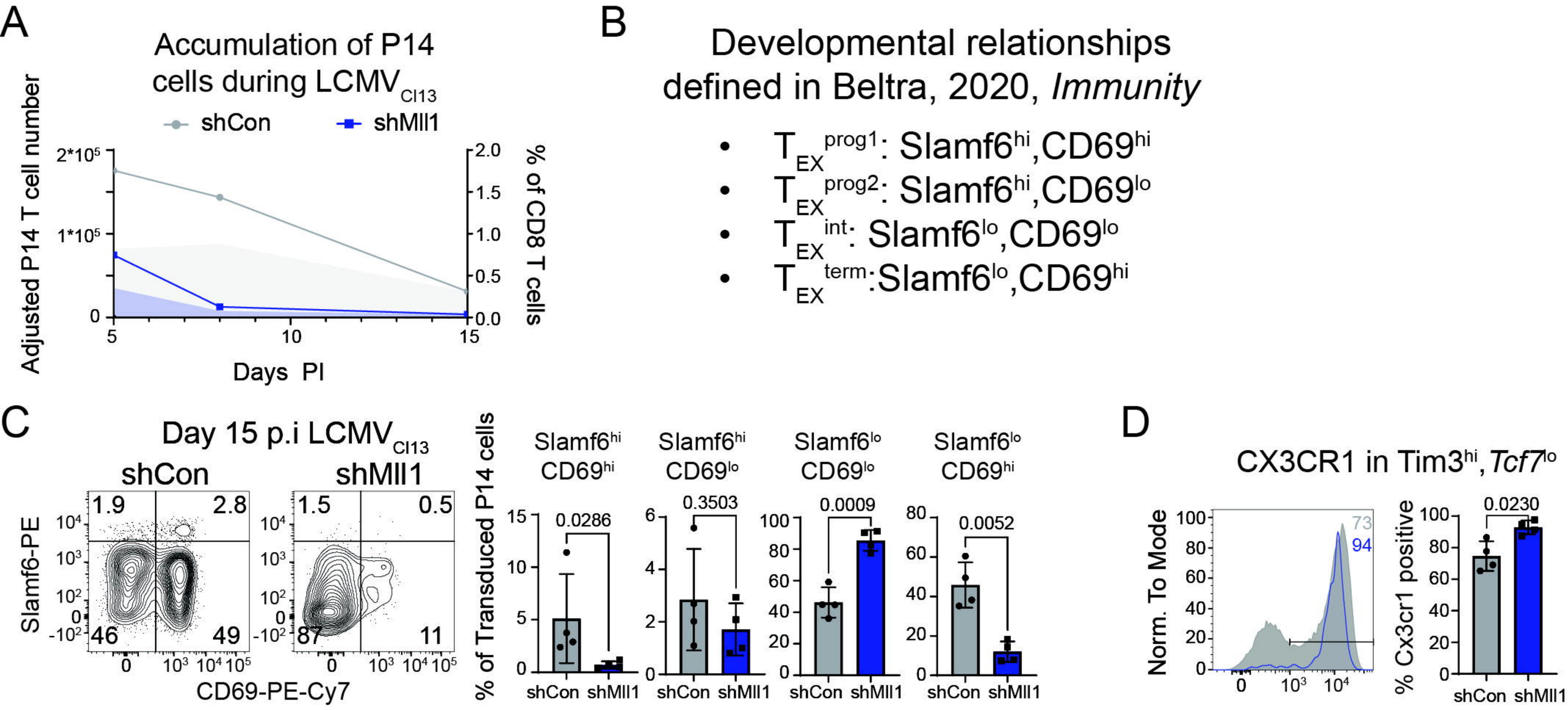
A
Accumulation of P14 cells during LCMV$_{Cl13}$
shCon
shMll1
Adjusted P14 T cell number
% of CD8 T cells
Days PI
B
Developmental relationships defined in Beltra, 2020, *Immunity*
T_{EX}^{prog1}: Slamf6^{hi},CD69^{hi}
T_{EX}^{prog2}: Slamf6^{hi},CD69^{lo}
T_{EX}^{int}: Slamf6^{lo},CD69^{lo}
T_{EX}^{term}:Slamf6^{lo},CD69^{hi}
C
Day 15 p.i LCMV$_{Cl13}$
shCon
shMll1
Slamf6-PE
CD69-PE-Cy7
% of Transduced P14 cells
Slamf6^{hi} CD69^{hi}
Slamf6^{hi} CD69^{lo}
Slamf6^{lo} CD69^{lo}
Slamf6^{lo} CD69^{hi}
0.0286
0.3503
0.0009
0.0052
D
CX3CR1 in Tim3^{hi},*Tcf7*^{lo}
Norm. To Mode
% Cx3cr1 positive
0.0230

Sup. Figure 5

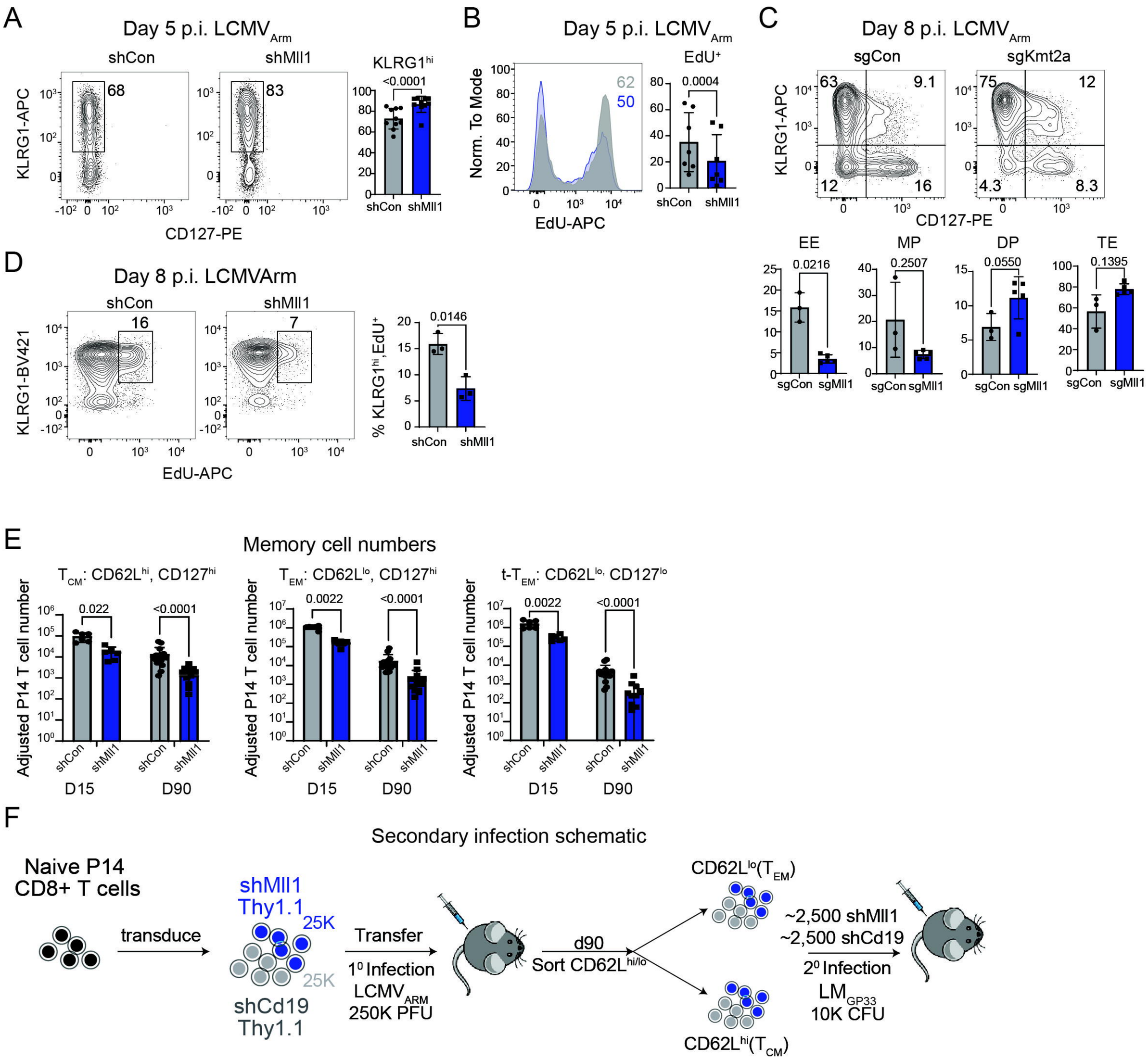
A
Day 5 p.i. LCMV Arm
shCon
shMll1
KLRG1-APC
CD127-PE
68
83
KLRG1hi
<0.0001
B
Day 5 p.i. LCMV Arm
Norm. To Mode
EdU-APC
62
50
EdU+
0.0004
C
Day 8 p.i. LCMV Arm
sgCon
sgKmt2a
63
9.1
12
16
75
12
4.3
8.3
EE
0.0216
MP
0.2507
DP
0.0550
TE
0.1395
sgMll1
D
Day 8 p.i. LCMVArm
KLRG1-BV421
16
7
% KLRG1hi,EdU+
0.0146
E
Memory cell numbers
TCM: CD62Lhi, CD127hi
TEM: CD62Llo, CD127hi
t-TEM: CD62Llo, CD127lo
Adjusted P14 T cell number
0.022
0.0022
D15
D90
F
Secondary infection schematic
Naive P14
CD8+ T cells
transduce
shMll1
Thy1.1
25K
shCd19
Thy1.1
Transfer
1⁰ Infection
LCMVARM
250K PFU
d90
Sort CD62Lhi/lo
CD62Llo(TEM)
CD62Lhi(TCM)
~2,500 shMll1
~2,500 shCd19
2⁰ Infection
LMGP33
10K CFU

Sup. Figure 6

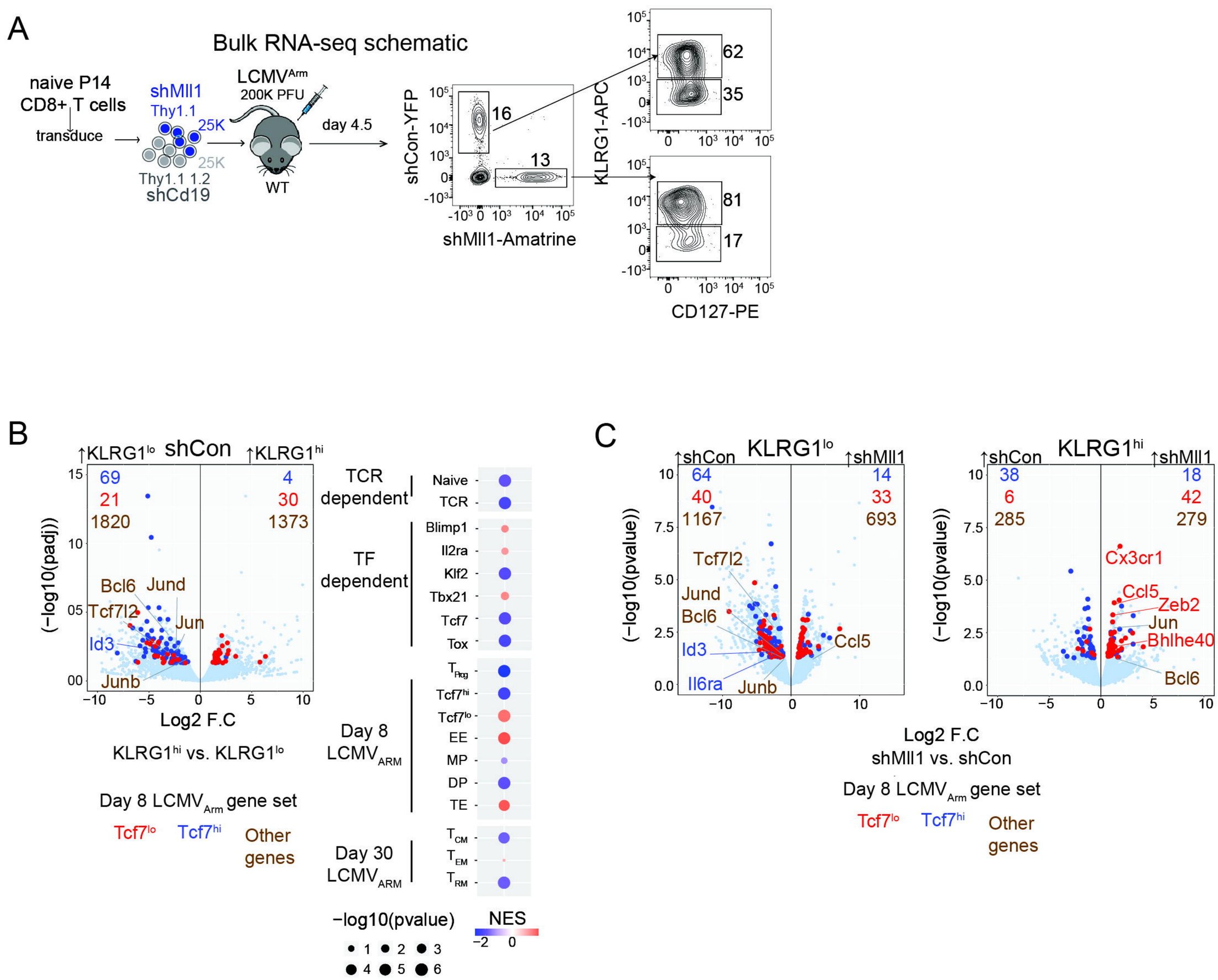
A
Bulk RNA-seq schematic
naive P14
CD8+ T cells
transduce
shMll1
Thy1.1
25K
25K
Thy1.1 1.2
shCd19
LCMV^Arm
200K PFU
WT
day 4.5
shCon-YFP
shMll1-Amatrine
16
13
KLRG1-APC
CD127-PE
62
35
81
17
B
↑KLRG1lo shCon ↑KLRG1hi
69
21
1820
4
30
1373
(−log10(padj))
Log2 F.C
Bcl6
Jund
Tcf7l2
Jun
Id3
Junb
KLRG1hi vs. KLRG1lo
Day 8 LCMVArm gene set
Tcf7lo
Tcf7hi
Other genes
TCR dependent
Naive
TCR
TF dependent
Blimp1
Il2ra
Klf2
Tbx21
Tcf7
Tox
Day 8 LCMVARM
TPrg
Tcf7hi
Tcf7lo
EE
MP
DP
TE
Day 30 LCMVARM
TCM
TEM
TRM
−log10(pvalue)
NES
C
KLRG1lo
↑shCon ↑shMll1
64
40
1167
14
33
693
Tcf7l2
Jund
Bcl6
Id3
Il6ra
Junb
Ccl5
KLRG1hi
38
6
285
18
42
279
Cx3cr1
Ccl5
Zeb2
Jun
Bhlhe40
Bcl6
(−log10(pvalue))
Log2 F.C
shMll1 vs. shCon
Day 8 LCMVArm gene set
Tcf7lo
Tcf7hi
Other genes

Sup. Figure 7

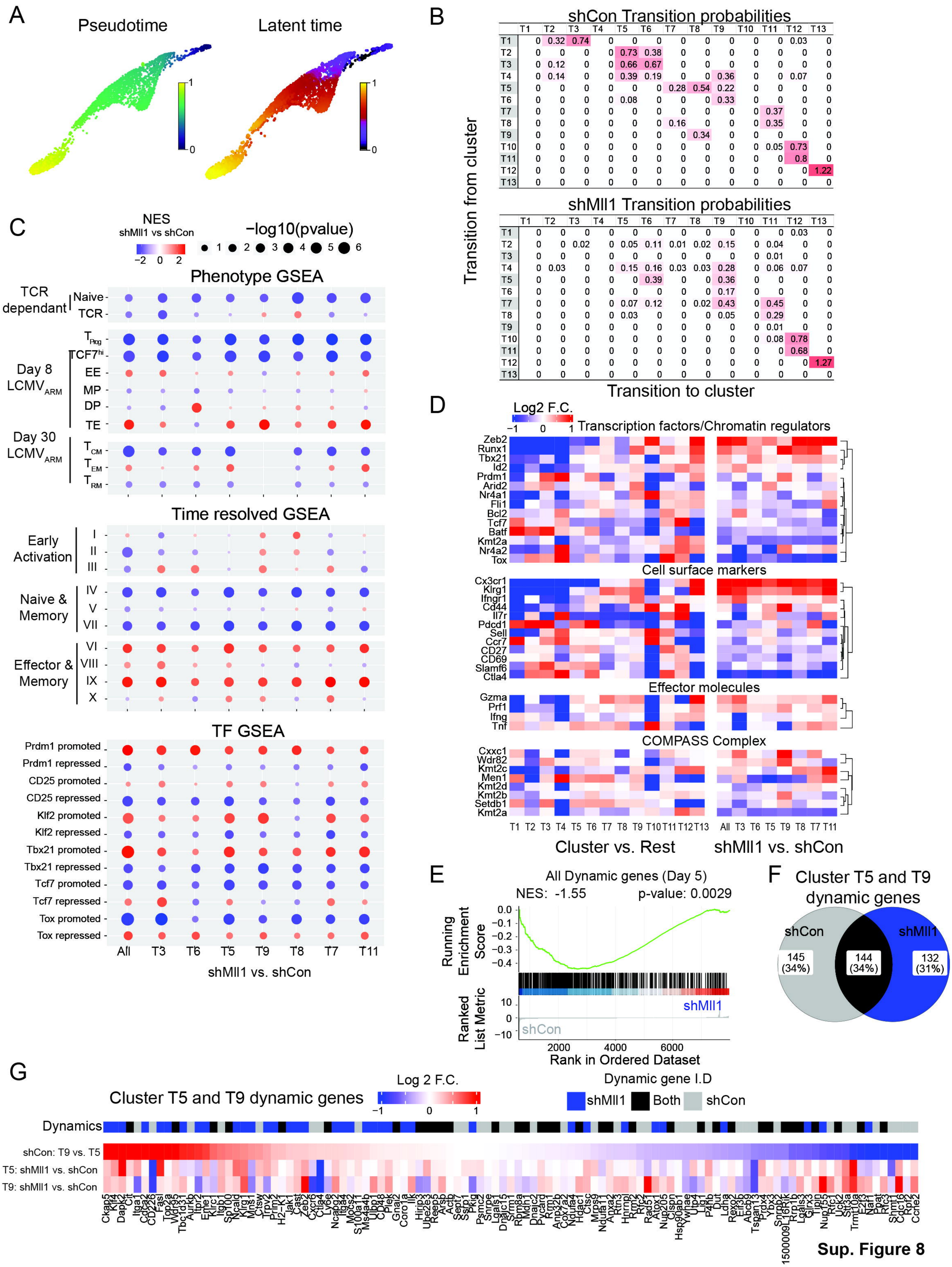
A
Pseudotime
Latent time
B
shCon Transition probabilities
shMll1 Transition probabilities
Transition from cluster
Transition to cluster
C
NES
shMll1 vs shCon
−log10(pvalue)
Phenotype GSEA
TCR dependant
Naive
TCR
Day 8 LCMV ARM
Day 30 LCMV ARM
Time resolved GSEA
Early Activation
Naive & Memory
Effector & Memory
TF GSEA
Prdm1 promoted
Prdm1 repressed
CD25 promoted
CD25 repressed
Klf2 promoted
Klf2 repressed
Tbx21 promoted
Tbx21 repressed
Tcf7 promoted
Tcf7 repressed
Tox promoted
Tox repressed
All T3 T6 T5 T9 T8 T7 T11
shMll1 vs shCon
D
Log2 F.C.
Transcription factors/Chromatin regulators
Cell surface markers
Effector molecules
COMPASS Complex
Cluster vs. Rest
shMll1 vs. shCon
E
All Dynamic genes (Day 5)
NES: -1.55
p-value: 0.0029
Running Enrichment Score
Ranked List Metric
shMll1
shCon
Rank in Ordered Dataset
F
Cluster T5 and T9 dynamic genes
shCon
shMll1
145 (34%)
144 (34%)
132 (31%)
G
Cluster T5 and T9 dynamic genes
Log 2 F.C.
Dynamic gene I.D
shMll1
Both
shCon
Dynamics
shCon: T9 vs. T5
T5: shMll1 vs. shCon
T9: shMll1 vs. shCon

Sup. Figure 8

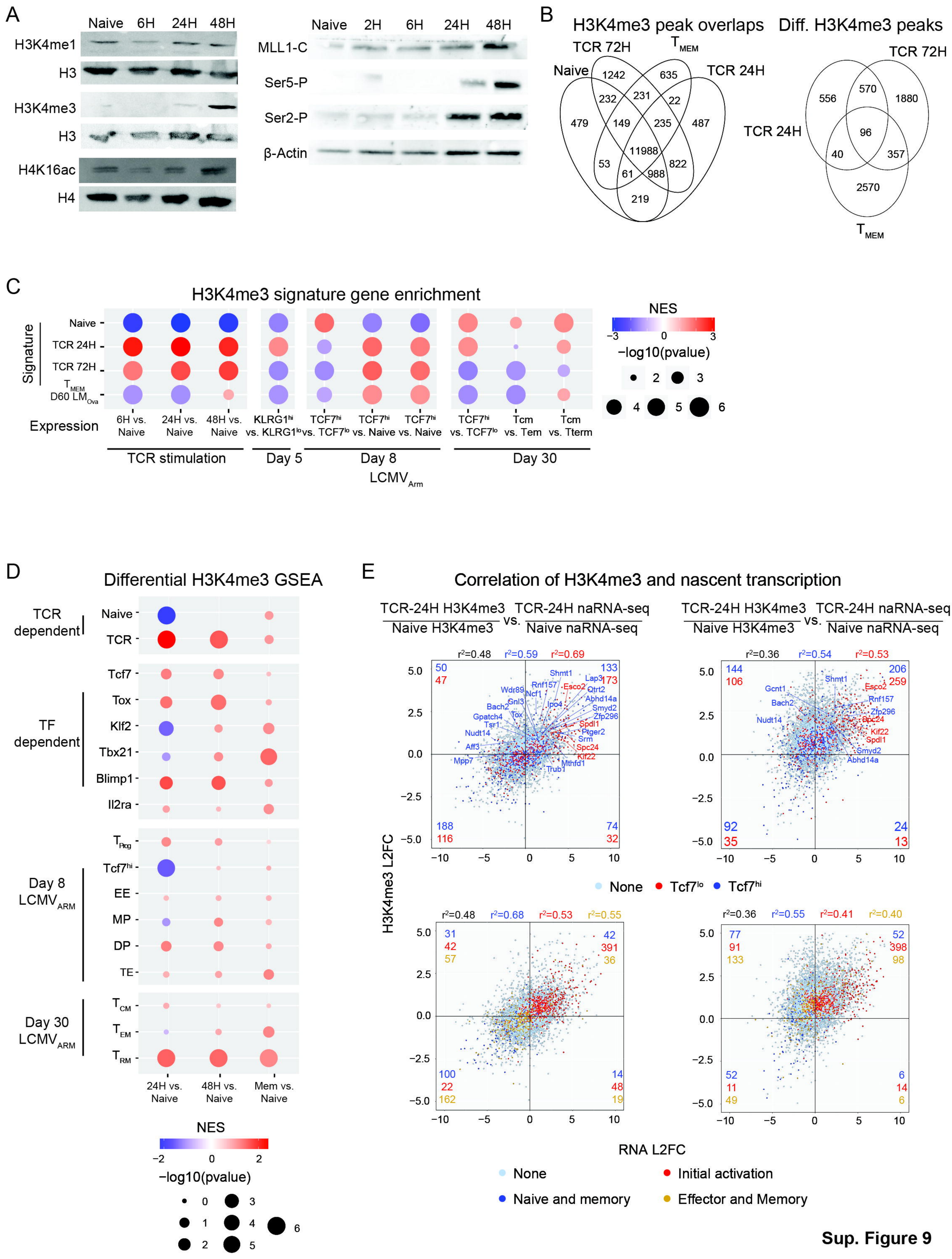
A
Naive 6H 24H 48H
H3K4me1
H3
H3K4me3
H3
H4K16ac
H4
Naive 2H 6H 24H 48H
MLL1-C
Ser5-P
Ser2-P
β-Actin
B
H3K4me3 peak overlaps
TCR 72H
T MEM
Naive
TCR 24H
1242
635
232
231
22
479
149
235
487
11988
53
822
61
988
219
Diff. H3K4me3 peaks
TCR 72H
556
570
1880
TCR 24H
96
40
357
2570
T MEM
C
H3K4me3 signature gene enrichment
Signature
Naive
TCR 24H
TCR 72H
T MEM
D60 LM Ova
Expression
6H vs. Naive
24H vs. Naive
48H vs. Naive
KLRG1hi vs. KLRG1lo
TCF7hi vs. TCF7lo
TCF7hi vs. Naive
TCF7hi vs. Naive
TCF7hi vs. TCF7lo
Tcm vs. Tem
Tcm vs. Tterm
TCR stimulation
Day 5
Day 8
LCMV Arm
Day 30
NES
−3 0 3
−log10(pvalue)
2 3
4 5 6
D
Differential H3K4me3 GSEA
TCR dependent
Naive
TCR
TF dependent
Tcf7
Tox
Klf2
Tbx21
Blimp1
Il2ra
T Prog
Day 8 LCMV ARM
Tcf7hi
EE
MP
DP
TE
Day 30 LCMV ARM
T CM
T EM
T RM
24H vs. Naive
48H vs. Naive
Mem vs. Naive
NES
−2 0 2
−log10(pvalue)
0 3
1 4 6
2 5
E
Correlation of H3K4me3 and nascent transcription
TCR-24H H3K4me3 / Naive H3K4me3 vs. TCR-24H naRNA-seq / Naive naRNA-seq
r2=0.48 r2=0.59 r2=0.69
50 47 133 173 188 116 74 32
Shmt1 Lap3 Rnf157 Esco2 Qtrt2 Wdr89 Ncf1 Abhd14a Gnl3 Ipo4 Smyd2 Bach2 Zfp296 Gpatch4 Tox Tsr1 Spdl1 Nudt14 Ptger2 Srm Aff3 Spc24 Kif22 Mpp7 Mthfd1 Trub1
TCR-24H H3K4me3 / Naive H3K4me3 vs. TCR-24H naRNA-seq / Naive naRNA-seq
r2=0.36 r2=0.54 r2=0.53
144 106 206 259 92 35 24 13
Shmt1 Esco2 Gcnt1 Rnf157 Bach2 Zfp296 Nudt14 Spc24 Kif22 Spdl1 Smyd2 Abhd14a
None Tcf7lo Tcf7hi
r2=0.48 r2=0.68 r2=0.53 r2=0.55
31 42 57 42 391 36 100 22 162 14 48 19
r2=0.36 r2=0.55 r2=0.41 r2=0.40
77 91 133 52 398 98 52 11 49 6 14 6
H3K4me3 L2FC
RNA L2FC
None
Initial activation
Naive and memory
Effector and Memory

Sup. Figure 9

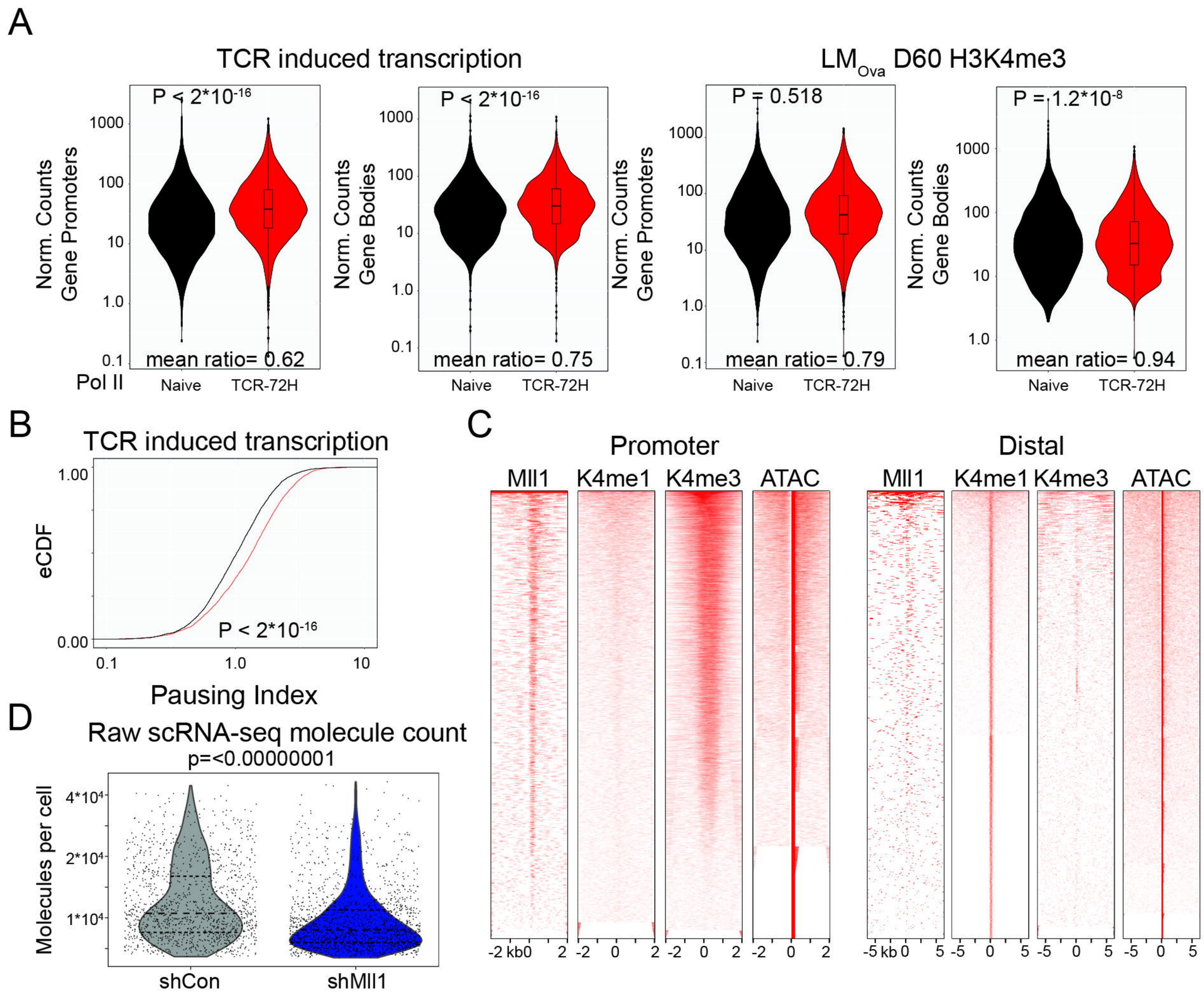

Sup. Figure 10